NASA TECHNICAL MEMORANDUM

NASA TM X-1155

C2

NASA TM X-1155

AERODYNAMIC CHARACTERISTICS OF A COMPLETE VTO LAUNCH VEHICLE AND REUSABLE FLYBACK CONFIGURATION FROM MACH 3.0 TO 6.0

by Robert J. McGhee

Langley Research Center
Langley Station, Hampton, Va.

NATIONAL AERONAUTICS AND SPACE ADMINISTRATION • WASHINGTON, D. C. • OCTOBER 1965

NASA TM X-1155

AERODYNAMIC CHARACTERISTICS OF A COMPLETE VTO LAUNCH VEHICLE AND REUSABLE FLYBACK CONFIGURATION FROM MACH 3.0 TO 6.0

By Robert J. McGhee

Langley Research Center
Langley Station, Hampton, Va.

NATIONAL AERONAUTICS AND SPACE ADMINISTRATION

AERODYNAMIC CHARACTERISTICS OF A COMPLETE VTO LAUNCH VEHICLE AND REUSABLE FLYBACK CONFIGURATION FROM MACH 3.0 TO 6.0*

By Robert J. McGhee
Langley Research Center

SUMMARY

An investigation has been conducted in the 2-foot hypersonic facility at the Langley Research Center to determine the longitudinal and lateral-directional stability for a vertical-take-off launch vehicle and its fixed-wing reusable first stage. Results have been compared with those of an exploratory investigation of a large winged vertical-take-off launch vehicle. In addition, control effectiveness and effects of vertical-tail arrangements and a semisubmerged flyback engine nacelle are indicated for the reusable first stage. The complete launch vehicle was tested at angles of attack from -10° to 16°, sideslip angles of 0° and 5°, and nominal Mach numbers of 3.0, 4.5, and 6.0. The reusable first stage was tested at angles of attack from -10° to 65° for the same Mach numbers and sideslip angles as the complete launch vehicle. Test Reynolds number per foot (0.305 meter) varied from approximately 1.0×10^6 to 2.2×10^6.

The results indicated that the longitudinal and the lateral center-of-pressure locations of the complete launch vehicle were well rearward of the estimated center-of-gravity location throughout the test Mach number range and for angles of attack from 0° to 16°. Longitudinal stability was indicated for the first-stage flyback configuration throughout the test Mach number and angle-of-attack ranges. Positive directional stability was obtained for the first-stage flyback configuration when both rudders were deflected outward 30°. Longitudinal control effectiveness decreased about 40 percent over the test Mach number range near maximum lift-drag ratio. Lateral control effectiveness decreased over the test Mach number range; however, only a nominal decrease occurred near maximum lift-drag ratio. Rudder reversal occurred near a Mach number of 4.5 for the first-stage reusable configuration; however, a significant improvement in directional stability was noted when both rudders were deflected outward 30°, and it is believed that positive rudder control over the test Mach number range would be obtained by differential deflections from this nominal 30°.

*Title, Unclassified.

INTRODUCTION

Winged reusable orbital launch vehicle systems may offer significant improvements from the standpoint of safety and reliability for future manned space flight missions. The NASA Langley Research Center has initiated a program to ascertain the nature and magnitude of the aerodynamic problems of vertical-take-off launch vehicle systems with fixed wings on the first stage.

The purpose of the present investigation was to determine aerodynamic characteristics of a complete two-stage vertical-take-off launch vehicle and its winged reusable first stage at Mach numbers from 3.0 to 6.0. Results of a similar investigation at Mach numbers of 2.36, 2.96, and 4.63 are presented in reference 1. An exploratory investigation of a winged reusable vehicle (ref. 2) indicated aerodynamic deficiencies in longitudinal, lateral, and directional stability. In order to improve the aerodynamic characteristics, the present investigation incorporated the following changes in the vehicle of reference 2: relocation of the wing resulting from a more detailed weight analysis of the probable vehicle center of gravity, change in planform of the wing, relocation and change in both planform and area of the vertical tails, and relocation of the flyback turbine engines. Some effects on the first-stage winged reusable configuration of vertical-tail arrangements and a semisubmerged flyback engine nacelle, together with the longitudinal, lateral, and directional control effectiveness, were examined at angles of attack up to about 50° to include maximum lift coefficients.

Tests were conducted on a 1/300-scale model of the complete launch vehicle in the 2-foot hypersonic facility at the Langley Research Center at angles of attack from approximately -10° to 65° at nominal Mach numbers of 3.0, 4.5, and 6.0. Data used in deriving stability characteristics were obtained at sideslip angles of 0° and 5°. The test Reynolds number per foot (0.305 meter) varied from approximately 1.0×10^{6} to 2.2×10^{6}.

SYMBOLS

Measurements for this investigation were taken in the U.S. Customary System of Units. Equivalent values are indicated herein parenthetically in the International System (SI) in the interest of promoting use of this system in future NASA reports. Details concerning the use of SI, together with physical constants and conversion factors, are given in reference 3.

The aerodynamic data are reduced to standard coefficient form. All data for the complete launch vehicle are referred to the body axes. All lateral-directional and control data for the first-stage winged reusable configuration are referred to the body axes, whereas the longitudinal data are referred to the stability axes. The moment reference for all data was selected to be 0.90 body diameter forward of the model base. All coefficients are referred to the body base area and body diameter.

C_N normal-force coefficient, $\frac{\text{Normal force}}{qS_{ref}}$

C_A axial-force coefficient, $\frac{\text{Total axial force}}{qS_{ref}}$

C_L lift coefficient, $\frac{\text{Lift}}{qS_{ref}}$

C_D drag coefficient, $\frac{\text{Total drag}}{qS_{ref}}$

C_m pitching-moment coefficient, $\frac{\text{Pitching moment}}{qS_{ref}d}$

C_l rolling-moment coefficient, $\frac{\text{Rolling moment}}{qS_{ref}d}$

C_n yawing-moment coefficient, $\frac{\text{Yawing moment}}{qS_{ref}d}$

C_Y side-force coefficient, $\frac{\text{Side force}}{qS_{ref}}$

C_{N_α} normal-force-curve slope, $\frac{\partial C_N}{\partial \alpha}$, per deg

C_{L_α} lift-curve slope, $\frac{\partial C_L}{\partial \alpha}$, per deg

$C_{m_{C_N}}$ longitudinal stability parameter (referred to body axes), $\frac{\partial C_m}{\partial C_N}$ at $C_N \approx 0$

$C_{m_{C_L}}$ longitudinal stability parameter (referred to stability axes), $\frac{\partial C_m}{\partial C_L}$ near $(L/D)_{max}$

C_{l_β} effective-dihedral parameter, $\frac{\Delta C_l}{\Delta \beta}$, per deg

C_{n_β} directional-stability parameter, $\frac{\Delta C_n}{\Delta \beta}$, per deg

C_{Y_β}	side-force parameter, $\frac{\Delta C_Y}{\Delta \beta}$, per deg
C_{m_δ}	longitudinal-control-effectiveness parameter, $\frac{\Delta C_m}{\Delta \delta_e}$, per deg where $\delta_e = \delta_{e,R} = \delta_{e,L}$
C_{l_δ}	lateral-control-effectiveness parameter, $\frac{\Delta C_l}{\Delta \delta_e}$, per deg where $\delta_e = \delta_{e,R} = -\delta_{e,L}$
C_{n_δ}	directional-control-effectiveness parameter, $\frac{\Delta C_n}{\Delta \delta_r}$, per deg
L/D	lift-drag ratio, $\frac{C_L}{C_D}$
c	local chord, ft (m)
$\bar{c}$	mean aerodynamic chord of exposed basic wing planform, ft (m)
d	body diameter, ft (m)
M	free-stream Mach number
p_t	stagnation pressure, atm (N/m^2)
q	free-stream dynamic pressure, lb/sq ft (N/m^2)
R	Reynolds number per foot (0.305 meter)
S_{ref}	model reference area, $\frac{\pi d^2}{4}$, sq ft (m^2)
t	local airfoil thickness, ft (m)
T_t	stagnation temperature, ^oF (^oK)
x,y	body coordinates (see fig. 2)
α	angle of attack, deg
β	angle of sideslip, deg
$\frac{x_{cg}}{d}$	center-of-gravity location forward of model base

$\frac{x_{cp}}{d}$ center-of-pressure location forward of model base

δ_e elevon deflection angle (positive when trailing edge is down), deg

δ_r rudder deflection angle (positive when trailing edge is to left), deg

θ_t vertical-tail toe-in angle, deg

Subscripts:

o conditions at zero angle of attack or zero lift

max maximum

R right

L left

MODEL DESCRIPTION

Two vehicle configurations were employed in this investigation: the complete two-stage launch vehicle and the winged reusable first stage. General model arrangements are shown in figure 1 and details in figure 2. Photographs of the launch vehicle and first-stage reusable configuration are shown in figure 3 and model dimensions are given in table I.

Complete Launch Vehicle

The complete launch vehicle model consisted of two stages in tandem as shown in figure 1. The first stage consisted of a ballistic rocket booster with a length-diameter ratio of 3.65 including interstage structure together with a wing and other reusable components to be described subsequently. The second stage consisted of an expendable booster with a length-diameter ratio of 2.92 including interstage structure. A representative ogival spacecraft having a length-diameter ratio of 2.21 including interstage structure was attached to the second stage. Two 15° half conical shrouds were designed to provide protection for the two upper rocket engines from aerodynamic loads during launch; the wing-body juncture fairing was shaped to provide protection for the two lower engines. However, no rocket engines were simulated on the model in this investigation. At the body base a short parabolic boattail fairing was incorporated. (See fig. 2(b).) Details of the spacecraft and shrouds are given in figures 2(a) and 2(b).

Winged Reusable First Stage

For the flyback configuration the second stage of the complete configuration was removed and a spherical forebody was attached to the ballistic first stage. Arrangements of the complete first-stage winged reusable configuration are shown in figure 1. Generally it consisted of two assemblies, the ballistic rocket booster and the winged reusable system attached thereto.

A trapezoidal wing (fig. 2(a)) with a 65° leading-edge sweep angle was mounted on the rocket booster so that the estimated center of gravity of the reusable first stage coincided with 22 percent of the exposed mean aerodynamic chord. The exposed planform area (neglecting trailing-edge extensions) was $7.5d^2$, the taper ratio was 0.35, and 5° of geometric dihedral was employed. The wing was mounted so that the uppermost wing element at the plane of symmetry was tangent to the body diameter - that is, the chord plane was parallel to and $t_{max}/2$ below the lowest body element. The basic airfoil section consisted of a symmetrical 10-percent-thick circular arc with a leading-edge radius of $t_{max}/6$ and a trailing-edge thickness of $t_{max}/3$; no twist or camber was incorporated. In order to improve subsonic L/D characteristics, a trailing-edge extension on the wing amounting to 15 percent of the local chord and consisting of a simple wedge profile was installed as shown in figure 2(a). At the center section, inboard of the 10-percent-semispan station, a center flap with a straight trailing edge amounting to 15 percent of the local chord at the 10-percent semispan station was provided.

The vertical tails (fig. 2(a)) were located outboard at the wing tips and employed 15° of outboard cant. Toe-in angles of 0° and 5° were provided by rotating the vertical tail about its midchord. The airfoil section was similar to that for the wing but without the trailing-edge extensions. The taper ratio was 0.60.

Two propulsion engine nacelles are under consideration for this flyback vehicle. One is a fully retractable nacelle and the other, a semisubmerged nacelle. At the test Mach numbers the vehicle would be in a hypersonic glide and the retractable nacelle was considered to be in the retracted position. Installation of the semisubmerged engine nacelle is shown in figure 1, and details are given in figure 2(b). A simple elliptic axisymmetrical pod to simulate a crew nacelle was located on the wing leading edge at 20 percent of the left wing semispan. It was mounted with its axis on the wing chord plane. (See figs. 1 and 2(a).)

Control Surfaces

Nearly full-span elevons amounting to 20 percent of the basic chord were provided. They extended from 10 percent to 90 percent of the exposed semispan (not including tip fairing). Deflection angles of 0° and ±20° were provided by means of hinge plates. The elevons were considered to provide both pitch and roll control.

Directional control was provided by control surfaces amounting to 30 percent of the basic chord. They were located on the trailing edge of the vertical tails and extended from approximately 10 percent of the tail height to the tip. By means of hinge plates, provisions were made for deflection angles of 0°, -10°, and $\pm 30^\circ$.

APPARATUS AND TESTS

The tests were conducted in the 2-foot hypersonic facility at the Langley Research Center, described in reference 4, at nominal Mach numbers of 3.0, 4.5, and 6.0, at angles of attack from -10° to 65°, and at angles of sideslip of 0° and 5°. The complete launch vehicle was tested at angles of attack from -10° to 16° and the winged reusable first stage at angles of attack from -10° to 65°. For the flyback configuration, longitudinal, lateral, and directional control deflections of -20°, $\pm 20^\circ$, and -10°, respectively, were used in the investigation. Test Reynolds number per foot (0.305 meter) varied from approximately 1.0×10^6 to 2.2×10^6. (See fig. 4.)

Six-component static aerodynamic force and moment measurements were obtained by means of an internally mounted strain-gage balance. All data were obtained with the model smooth - that is, no transition strips were used. Angles of attack and sideslip were corrected for balance and sting deflection under load. All drag data have been presented with no base-pressure corrections applied. All lateral and directional summary data have been calculated by using the actual angle of sideslip at each angle of attack. The average test conditions and Reynolds number variation during the launch trajectory are as follows:

Mach number, M	Stagnation temperature, T_t, $^\circ F$ ($^\circ K$)	Stagnation pressure, p_t, atm (kN/m^2)		Reynolds number for complete launch vehicle (based on overall length)	
		Complete launch vehicle	Reusable first stage	Test	Flight
3.0	100 (311.11)	1.0 (101.3)	0.46 (46.6)	2.6×10^6	1.6×10^6
4.5	300 (422.22)	1.8 (182.4)	1.6 (162.1)	1.4×10^6	$.22 \times 10^6$
6.0	300 (422.22)	3.4 (344.5)	3.4 (344.5)	1.4×10^6	$.007 \times 10^6$

RESULTS AND DISCUSSION

The results of this investigation have been divided into two primary parts. The first consists of the data for the complete launch vehicle; the second, the data for the winged reusable first stage. Figures 5 to 8 present the basic and summary aerodynamic characteristics of the complete launch configuration. Figures 9 to 15 include the basic and summary data for the winged reusable first

stage. All force and moment data are referred to the assumed center of gravity which was 0.90 diameter forward of the model base and which is the estimated center of gravity for the reusable first stage during flyback to the recovery site.

Complete Launch Vehicle

Figures 6 and 7(a) show the complete launch vehicle to be both longitudinally and directionally unstable about the chosen moment reference. In order to assess the longitudinal and directional stability adequately, however, consideration must be given to the actual center of gravity and its change during launch as fuel is progressively consumed. An estimate of the center-of-gravity location at the representative test Mach numbers is shown in figure 8. Figure 8 shows that the longitudinal and the lateral center-of-pressure locations of the launch vehicle are rearward of the estimated center-of-gravity location for all test Mach numbers at an angle of attack of 0°; therefore, positive longitudinal stability and directional stability are indicated. The data indicate the same results up to maximum test angles of attack of 16°.

Winged Reusable First Stage

Longitudinal stability characteristics.- Comparison of the data for the vehicle of reference 2 and the present vehicle shows the large improvements obtained in longitudinal stability near maximum L/D. (See fig. 10.) This improvement can be attributed to a change in wing planform coupled with a rearward shift of the wing. Removal of the vertical tails resulted in significant decrements in stability throughout the Mach number range. However, all the results for the present first-stage flyback configuration indicate positive longitudinal stability $\left(-C_{m_{C_L}}\right)$ throughout the test Mach number and angle-of-attack ranges. The configuration with both rudders deflected outward 30° had the highest longitudinal stability over the test Mach number range, and the 30° deflection of the rudders is subsequently shown to be desirable for directional stability as well. Figure 9(b) indicates that installation of the semisubmerged engine nacelle provided an increase in the pitching-moment level in the low angle-of-attack range but resulted in a more severe stable break in the pitching-moment curves in the high angle-of-attack range. This effect was probably caused by high positive pressures resulting from strong shock waves on the forward facing ramp, employed to close the engine inlets.

The improvements in $(L/D)_{max}$, especially at the higher Mach numbers, are shown in figure 10. The vehicle of reference 2 indicates values of $(L/D)_{max}$ of about 1.60 and 1.27 at $M = 3.0$ and $M = 6.0$, respectively; whereas, the present vehicle indicates values of $(L/D)_{max}$ of about 1.61 and 1.40 at $M = 3.0$ and $M = 6.0$, respectively. Installation of the semisubmerged engine nacelle resulted in small degradation in $(L/D)_{max}$ due to increased pressure drag associated with the additional volume of the engine nacelle.

Lateral-directional stability characteristics.- Figure 12 indicates that about the same amount of lateral instability exists for both the vehicle of

reference 2 and the present vehicle at $\alpha = 0^\circ$. Positive effective dihedral $\left(-C_{l_\beta}\right)$, however, is shown for the present vehicle at angles of attack above 10° and up to about 50° to include maximum lift coefficients. (See fig. 11.)

Figure 12 shows the substantial improvement in directional stability of the present vehicle over the vehicle of reference 2 at 0° angle of attack; however, a small amount of directional instability remains. Wing-tip-mounted vertical tails employing 15° of outboard cant and 5° of toe-in coupled with an increase in vertical-tail area of about 25 percent account for the improvement in C_{n_β}. Positive directional stability $\left(C_{n_\beta}\right)$ was obtained for the present configuration when both rudders were deflected outward 30° for the low and moderate angles of attack including $\alpha = 20^\circ$ (near maximum L/D). Directional stability deteriorated rapidly at the higher angles of attack.

Control effectiveness.- Figure 15 summarizes the control effectiveness at Mach numbers from 3.0 to 6.0. The data show that longitudinal control effectiveness $\left(C_{m_\delta}\right)$ increased rapidly with increasing angle of attack up to $\alpha = 50^\circ$ (near maximum C_L). Appreciable decreases with Mach number are shown for both $\alpha = 0^\circ$ and $\alpha = 20^\circ$ (near maximum L/D); at $\alpha = 50^\circ$ (near maximum C_L), this trend reversed. For example, at $\alpha = 20^\circ$, longitudinal control effectiveness decreased about 40 percent from $M = 3.0$ to $M = 6.0$. Figure 15 also shows similar trends for lateral control effectiveness $\left(C_{l_\delta}\right)$; however, the degradation with Mach number near maximum L/D ($\alpha = 20^\circ$) is shown to be relatively small. Serious difficulties are indicated by the directional-control-effectiveness curves in that for the rudder deflection used to derive these results ($\delta_r = -10^\circ$) a control reversal is shown near $M = 4.5$ for the moderate and high angles of attack. Even for $\alpha = 0^\circ$ essentially no rudder control is indicated at this Mach number. In reference 1, rudder effectiveness was shown to decrease with increasing Mach number up to the maximum test Mach number of that investigation, $M = 4.63$. As stated previously, however, a significant improvement in directional stability was noted in the present investigation when both rudders were deflected outward 30° (see fig. 12), and it is believed that differential deflections from this nominal 30° would provide positive directional control at all test Mach numbers.

CONCLUDING REMARKS

An investigation has been conducted in the 2-foot hypersonic facility at the Langley Research Center to determine the longitudinal and lateral-directional stability of a complete launch vehicle and its fixed-wing reusable first stage. Results have been compared with those of an exploratory investigation of a large winged vertical-take-off reusable launch vehicle. In addition, control effectiveness was obtained for the reusable first stage. Data were obtained at Mach numbers from 3.0 to 6.0, angles of attack from -10° to 65°, and sideslip angles of 0° and 5°. Test Reynolds number per foot (0.305 meter)

varied from approximately 1.0×10^6 to 2.2×10^6. The following concluding remarks are considered appropriate:

1. The longitudinal and the lateral center-of-pressure locations of the complete launch vehicle were rearward of the estimated center-of-gravity location throughout the test Mach number range and for angles of attack from 0° to 16°.

2. Positive longitudinal stability was indicated for the first-stage flyback configuration throughout the test Mach number and angle-of-attack ranges.

3. Positive directional stability was obtained for the first-stage flyback configuration when both rudders were deflected outward 30°.

4. Near maximum lift-drag ratio, longitudinal control effectiveness decreased about 40 percent over the test Mach number range.

5. Lateral control effectiveness decreased over the test Mach number range; however, near maximum lift-drag ratio only a nominal decrease occurred.

6. Rudder reversal occurred near a Mach number of 4.5 for the first-stage reusable configuration; however, a significant improvement in directional stability was noted when both rudders were deflected outward 30°, and it is belived that positive rudder control over the test Mach number range would be obtained by differential deflections from this nominal 30°.

Langley Research Center,
National Aeronautics and Space Administration,
Langley Station, Hampton Va., June 11, 1965.

REFERENCES

1. McGhee, Robert J.; and Pierpont, P. Kenneth: Supersonic Characteristics of Both Launch and Flyback Configurations of a VTO Reusable Launch Vehicle. NASA TM X-1095, 1965.

2. Pierpont, P. Kenneth: Investigation of a Large Winged First Stage of a VTO Reusable Orbital Launch Vehicle from Mach 2.3 to 6.0. NASA TM X-1116, 1965.

3. Mechtly, E. A.: The International System of Units - Physical Constants and Conversion Factors. NASA SP-7012, 1964.

4. Stokes, George M.: Description of a 2-Foot Hypersonic Facility at the Langley Research Center. NASA TN D-939, 1961.

TABLE I.- GEOMETRIC CHARACTERISTICS

Reusable first-stage configuration -	
Body:	
Length, overall, in. (cm)	5.48 (13.92)
Diameter, in. (cm)	1.32 (3.35)
Base area, sq in. (cm^2)	1.37 (8.80)
Length/Diameter, cylindrical body	3.65
Moment reference from base, in. (cm)	1.19 (3.02)
Shrouds:	
Length, 15° conical, in. (cm)	1.05 (2.67)
Wing:	
Total area, including trailing-edge extension, sq in. (cm^2)	21.28 (137.30)
Exposed area, including trailing-edge extension, sq in. (cm^2)	15.28 (98.60)
Exposed area, neglecting trailing-edge extension, sq in. (cm^2)	13.09 (84.50)
Root chord at fuselage juncture, in. (cm)	3.91 (9.93)
Tip chord, in. (cm)	1.37 (3.48)
Span (total), in. (cm)	6.27 (15.93)
Leading-edge sweep, deg	65
Positive dihedral, deg	5
$(t/c)_{max}$	0.10
Leading-edge radius	$t_{max}/6$
Trailing-edge thickness	$t_{max}/3$
Airfoil section	Circular arc
$\bar{c}$, based on exposed area, in. (cm)	2.85 (7.24)
Moment reference, from leading-edge wing	$0.22\bar{c}$
Moment reference, distance from body base, in. (cm)	1.19 (3.02)
Aspect ratio, design	2.08
Vertical tail:	
Area, each, sq in. (cm^2)	1.64 (10.60)
Root chord, in. (cm)	1.52 (3.86)
Tip chord, in. (cm)	0.91 (2.31)
Height, in. (cm)	1.35 (3.43)
Leading-edge sweep, deg	30
$(t/c)_{max}$	0.10
Leading-edge radius	$t_{max}/6$
Trailing-edge thickness	$t_{max}/3$
Airfoil section	Circular arc
Toe-in, deg	0 and 5
Cant, deg	15
Tail moment arm, c.g. to $(\bar{c}/4)$ tail, in. (cm)	3.13 (7.95)
Second-stage expendable rocket booster -	
Length, in. (cm)	3.85 (9.78)
Diameter, in. (cm)	1.32 (3.35)
Length/Diameter	2.92
Spacecraft -	
Length, in. (cm)	2.92 (7.42)
Diameter, base, in. (cm)	1.32 (3.35)
Length/Diameter	2.21

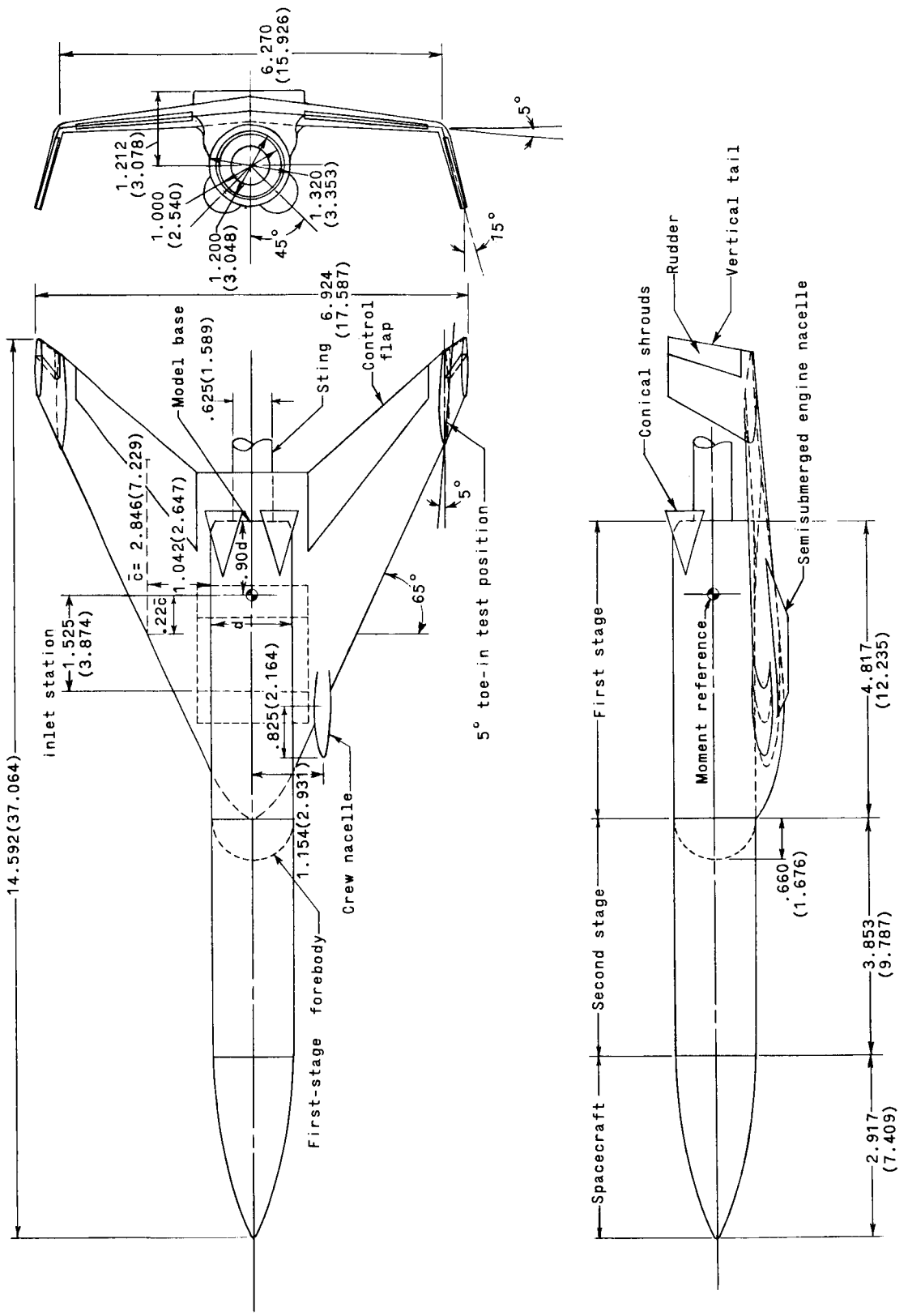

Figure 1.- Arrangement and geometric details of the launch vehicle with a fixed-wing reusable first stage. Dimensions are given first in inches and parenthetically in centimeters.

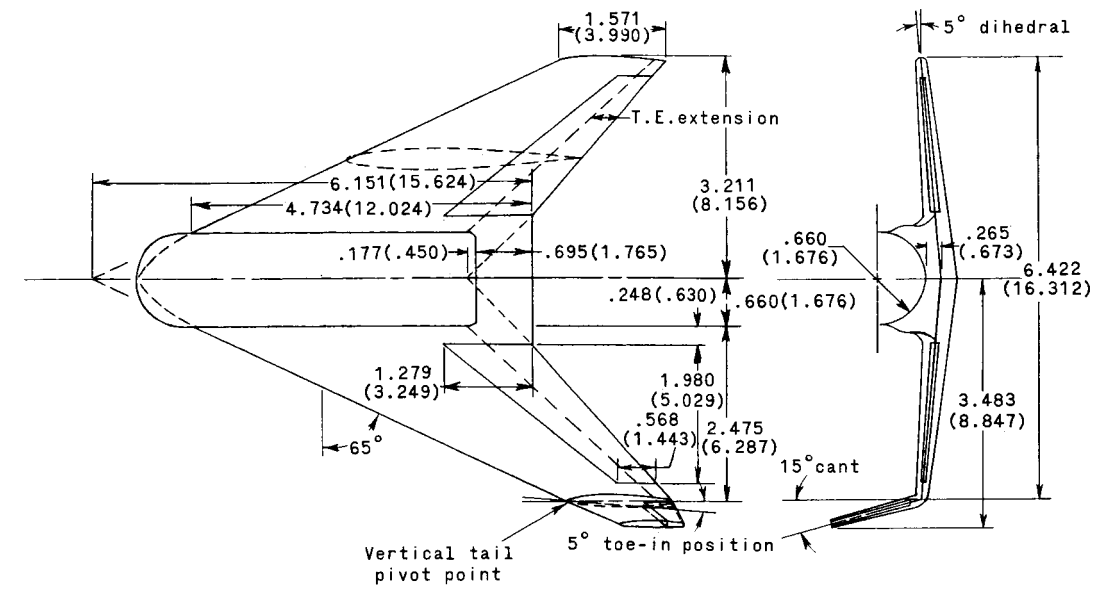

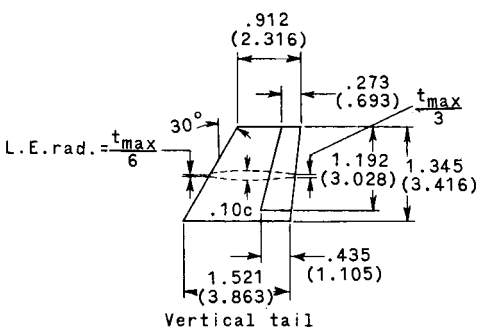

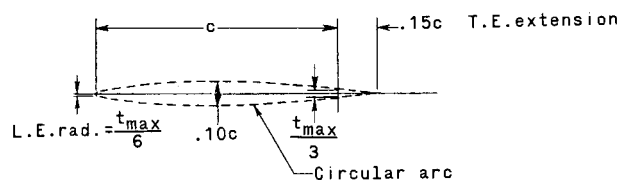

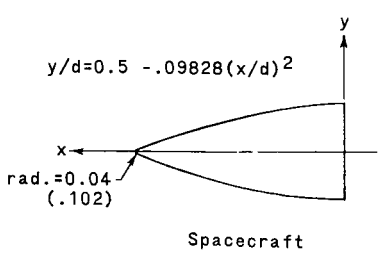

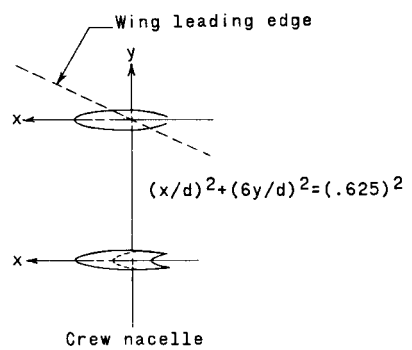

(a) Wing, vertical tail, crew nacelle, and spacecraft.

Figure 2.- Details of model components. Dimensions are given first in inches and parenthetically in centimeters.

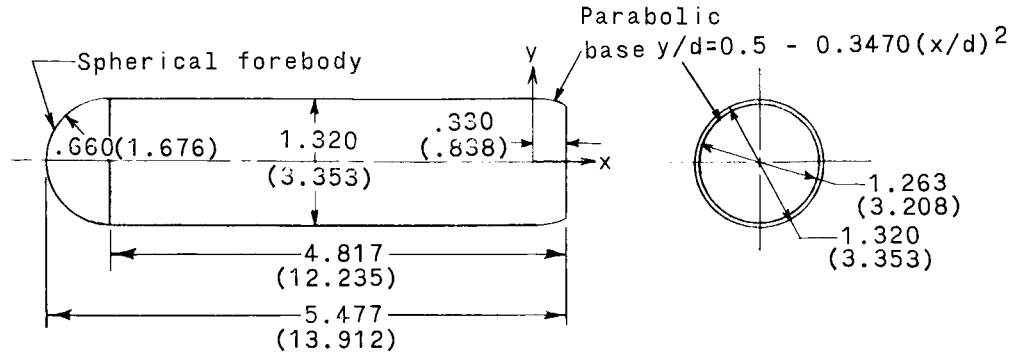

Body alone

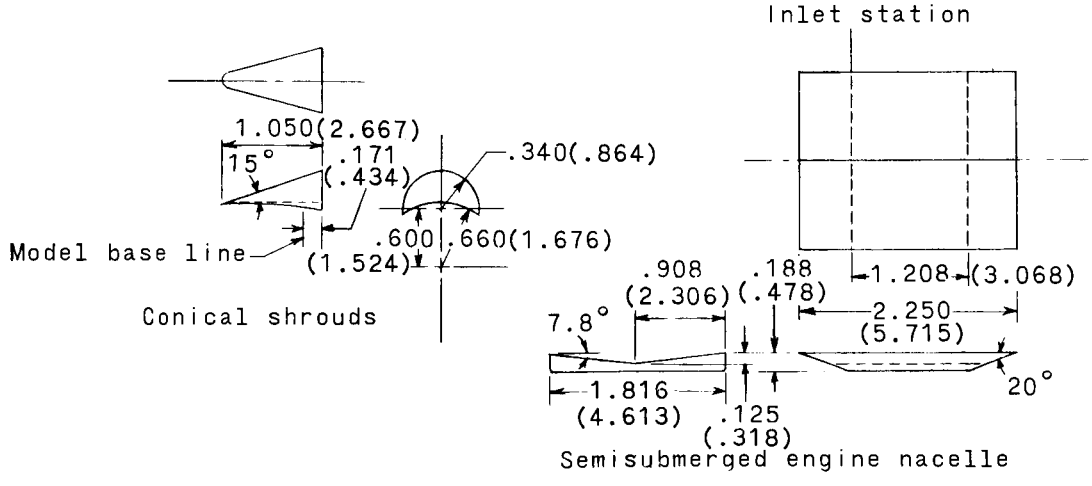

(b) Body alone, conical shrouds, forebody and base arrangement, and flyback engine nacelle.

Figure 2.- Concluded.

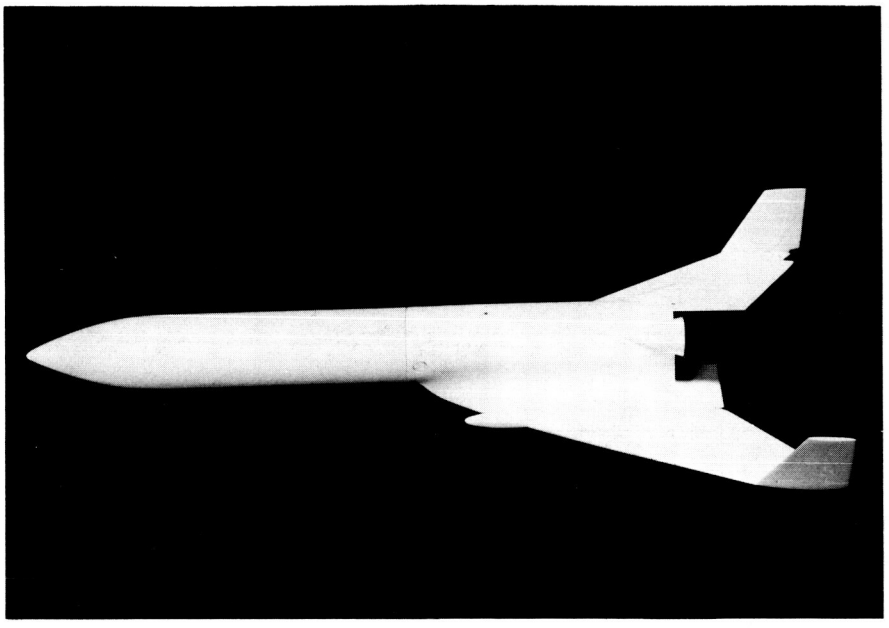

(a) Complete launch configuration. L-65-797

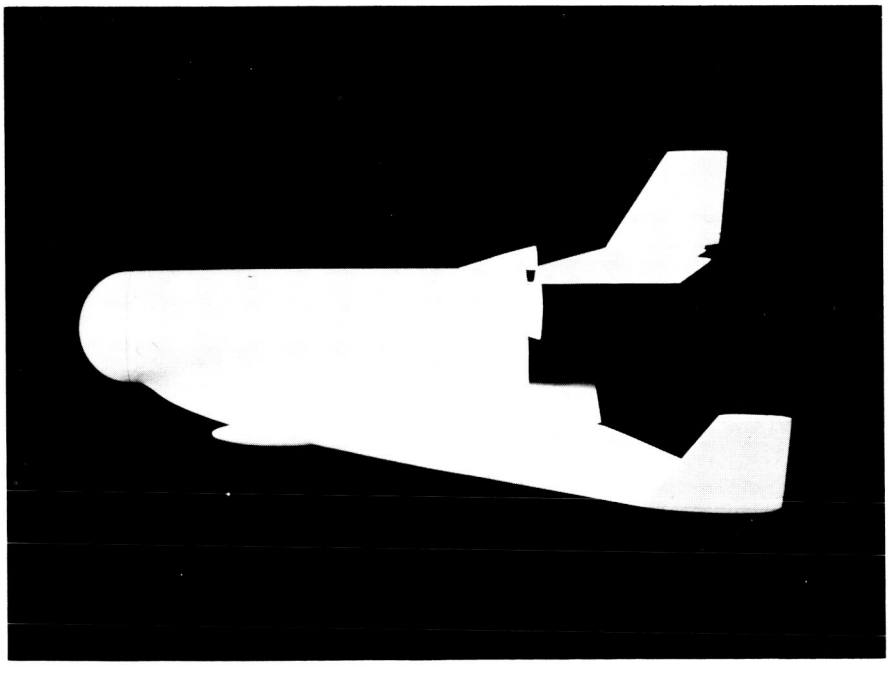

(b) First-stage reusable configuration. L-65-798

Figure 3.- Photographs of models used in the investigation.

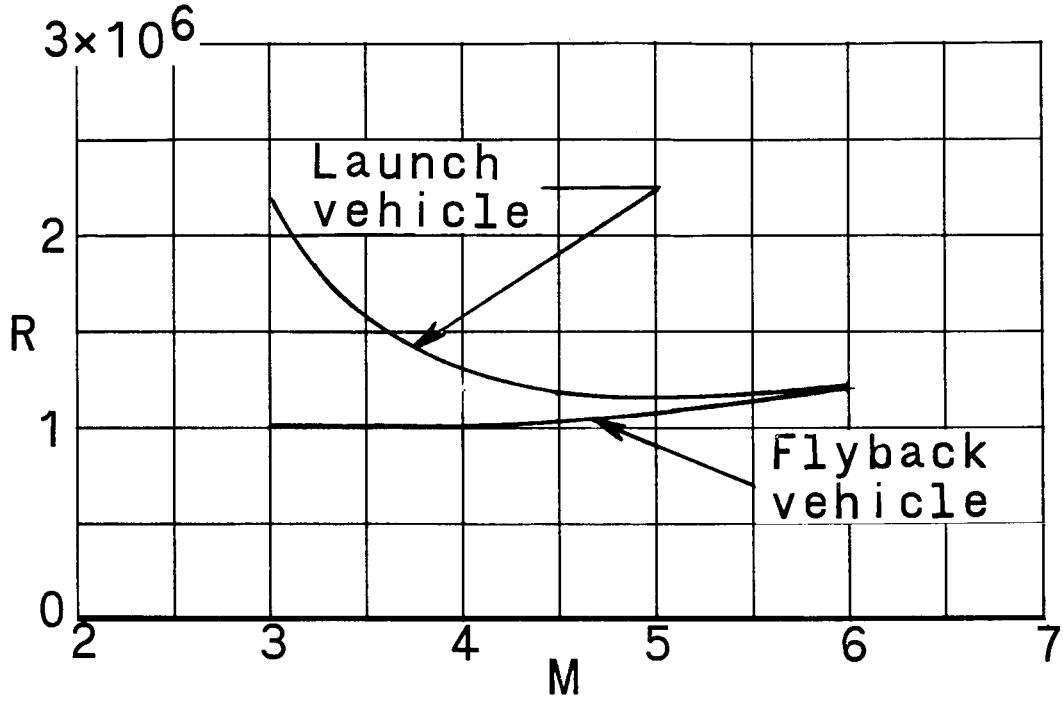

Figure 4.- Variation with Mach number of the test Reynolds number per foot (0.305 meter).

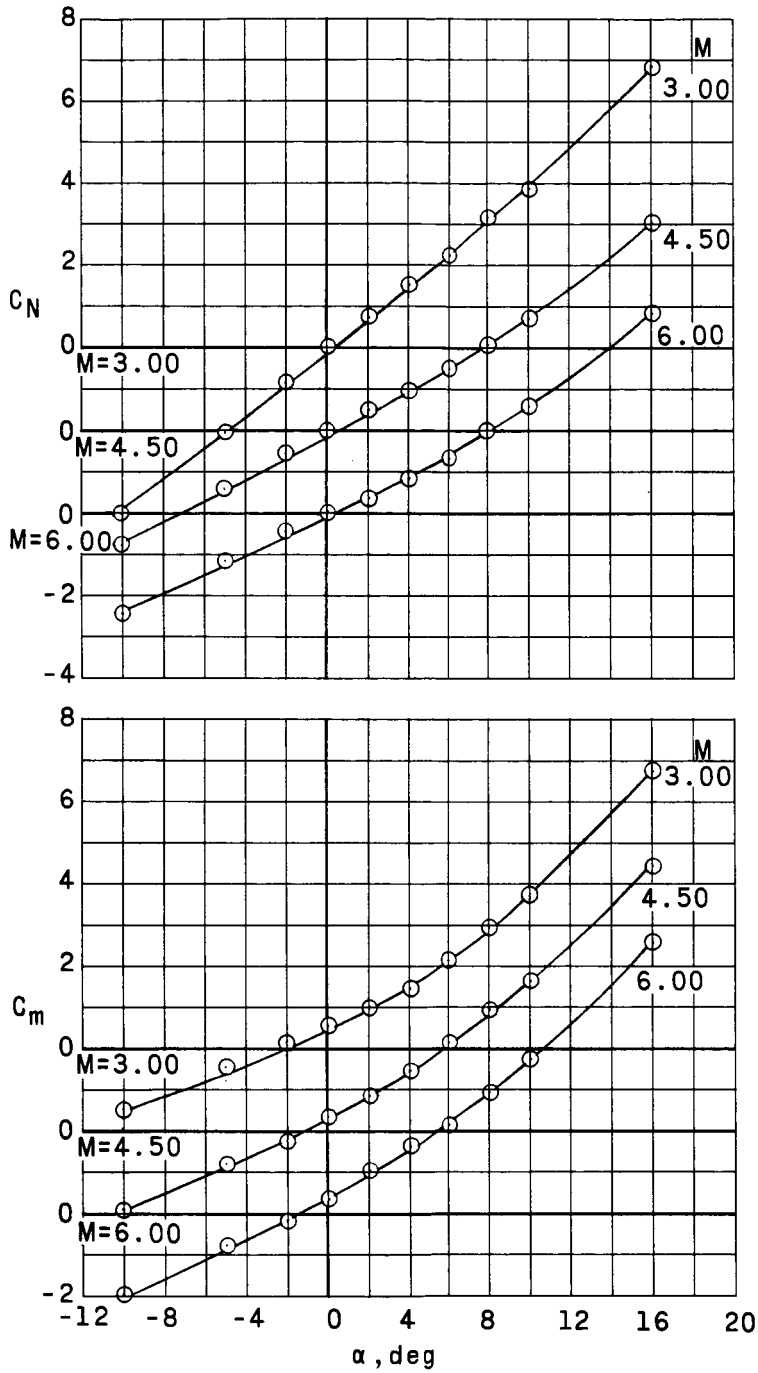

(a) C_N and C_m plotted against α.

Figure 5.- Longitudinal aerodynamic characteristics of the complete launch vehicle. Engine nacelle off; $\theta_t = 5^0$; $\beta = 0^0$.

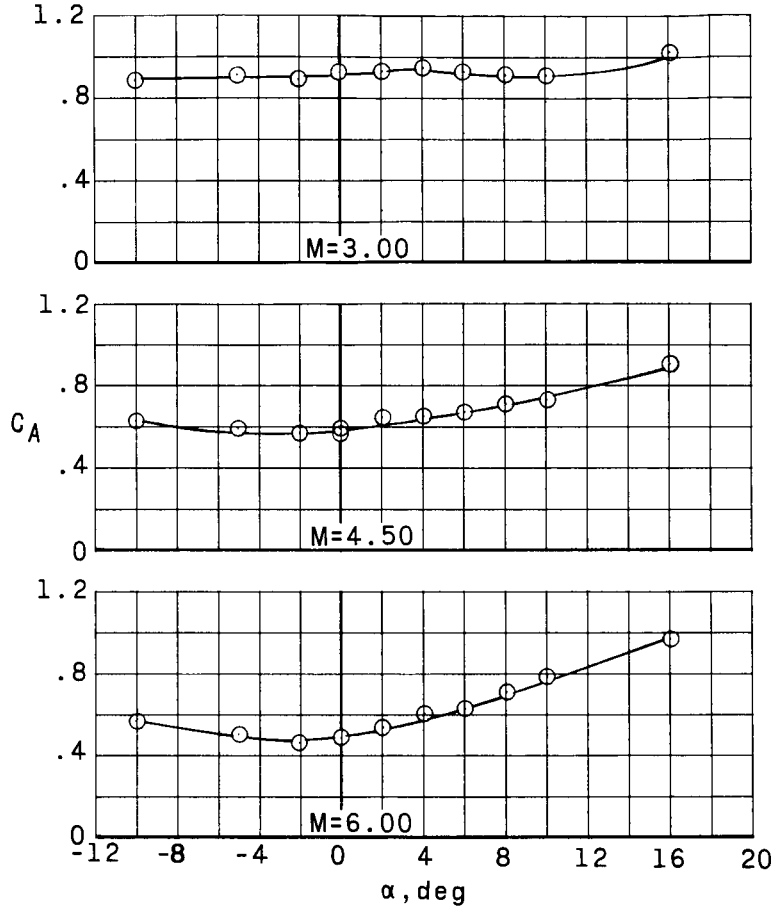

(b) C_A plotted against α.

Figure 5.- Concluded.

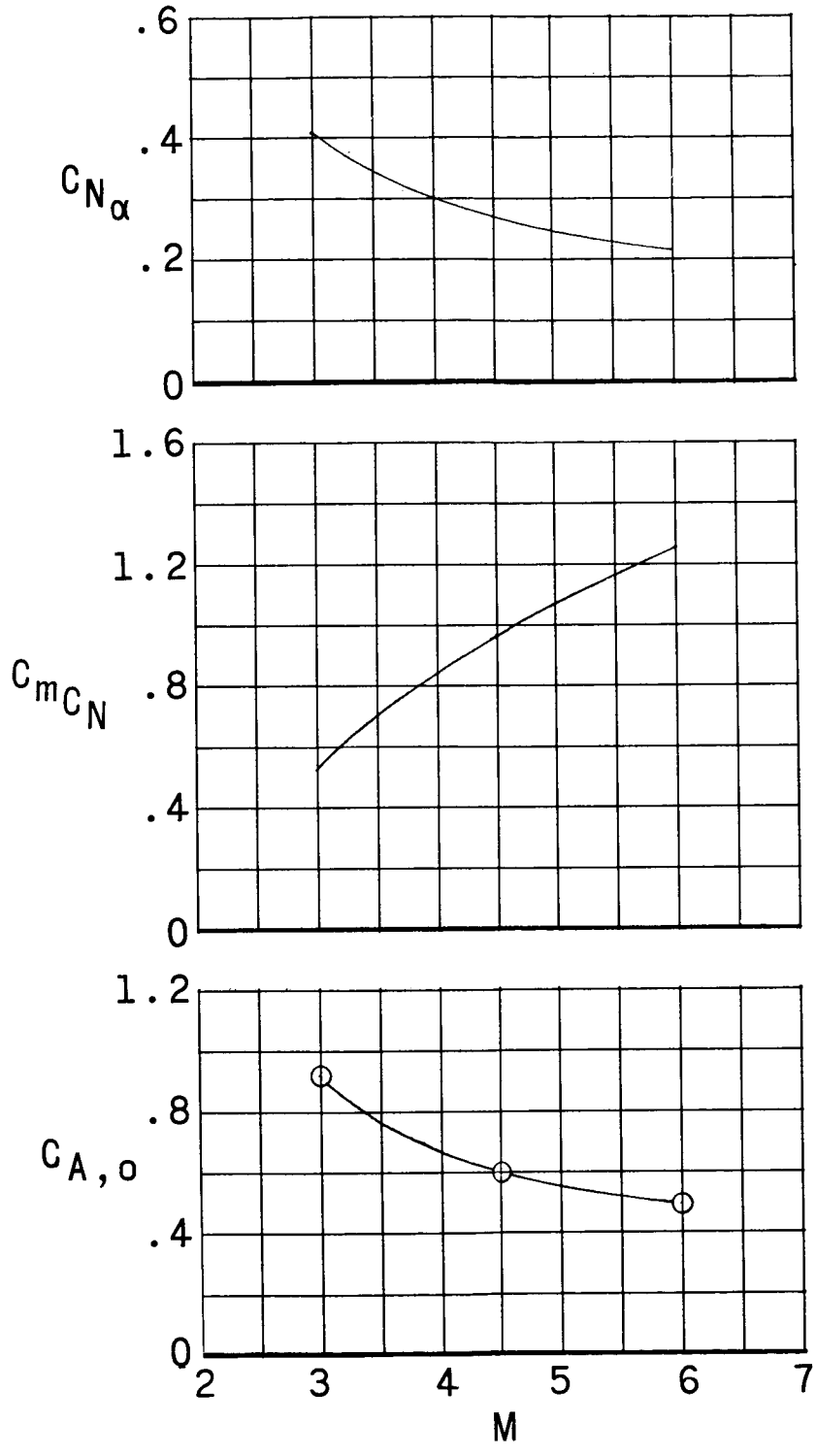

Figure 6.- Variation with Mach number of the longitudinal-stability and drag parameters for the complete launch vehicle. Engine nacelle off; $\theta_t = 5^0$; $\beta = 0^0$.

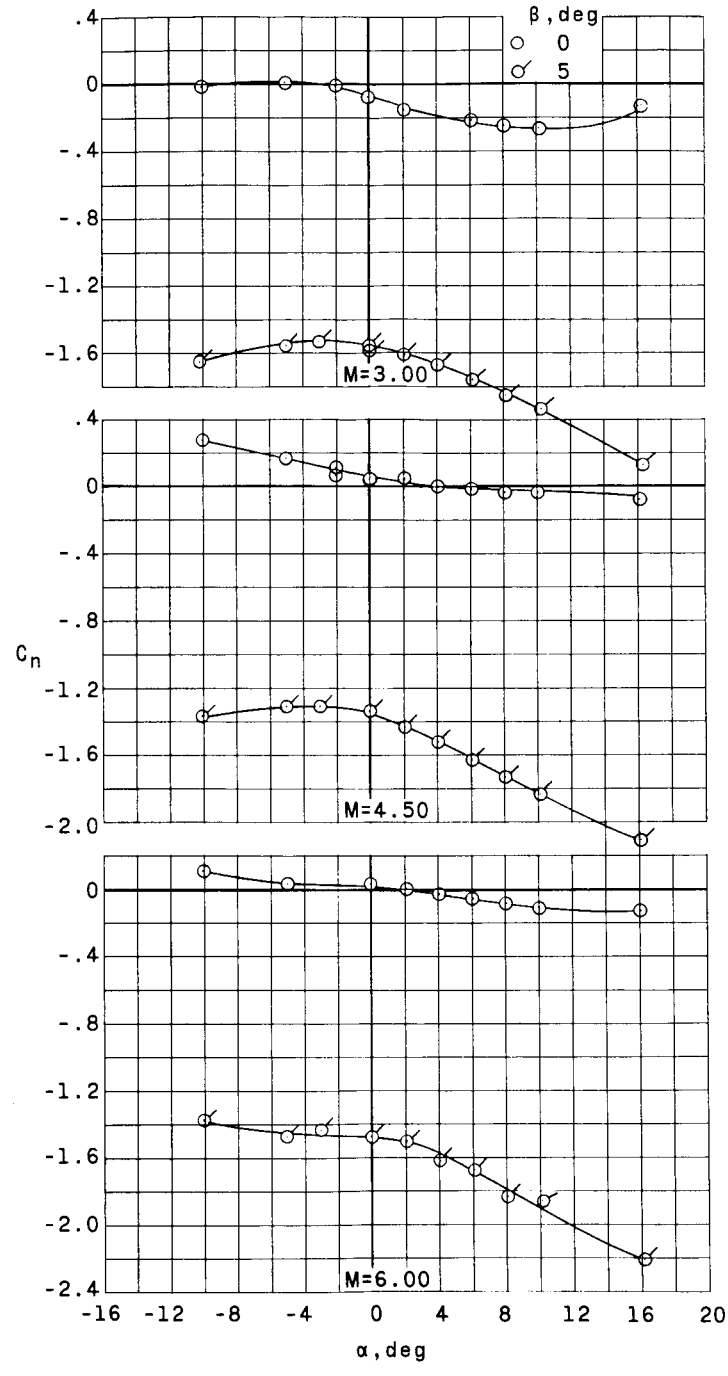

(a) C_n plotted against α.

Figure 7.- Lateral aerodynamic characteristics of the complete launch vehicle. Engine nacelle off; $\theta_t = 5^0$.

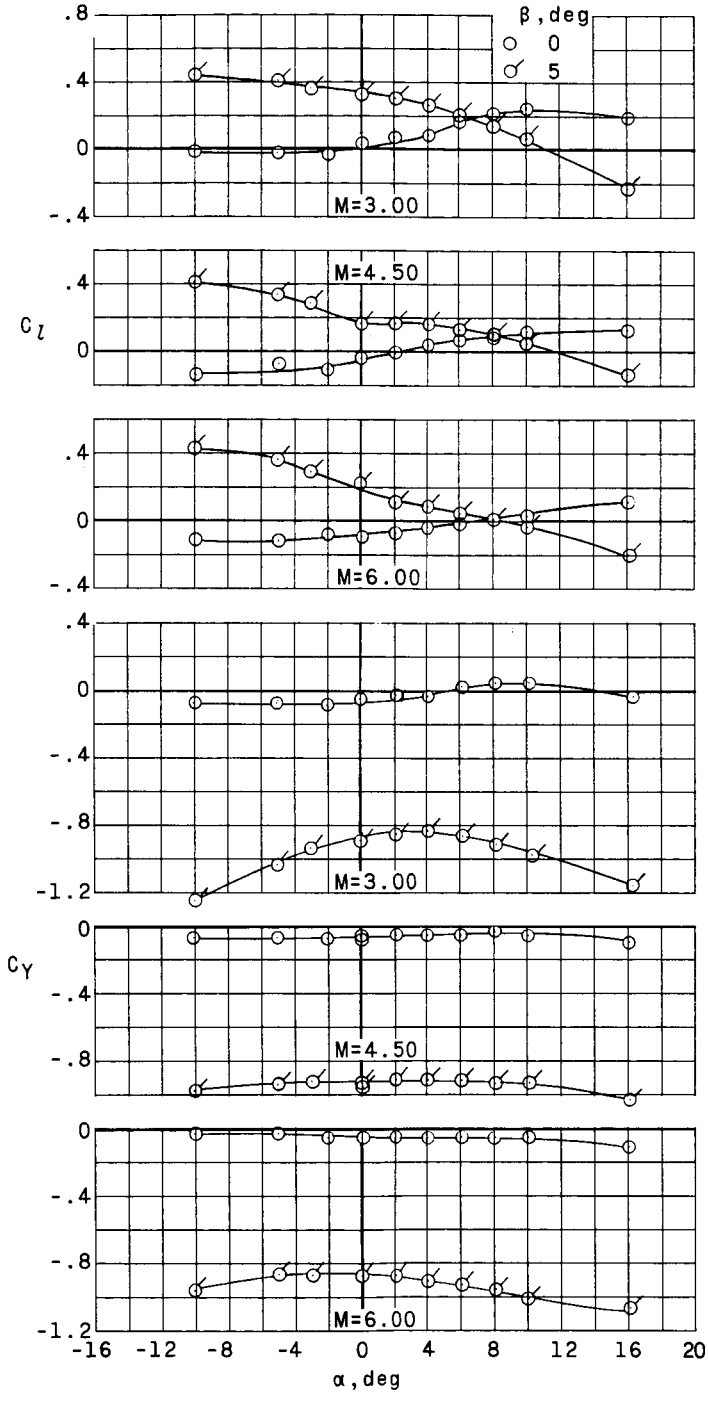

(b) C_l and C_Y plotted against α.

Figure 7.- Concluded.

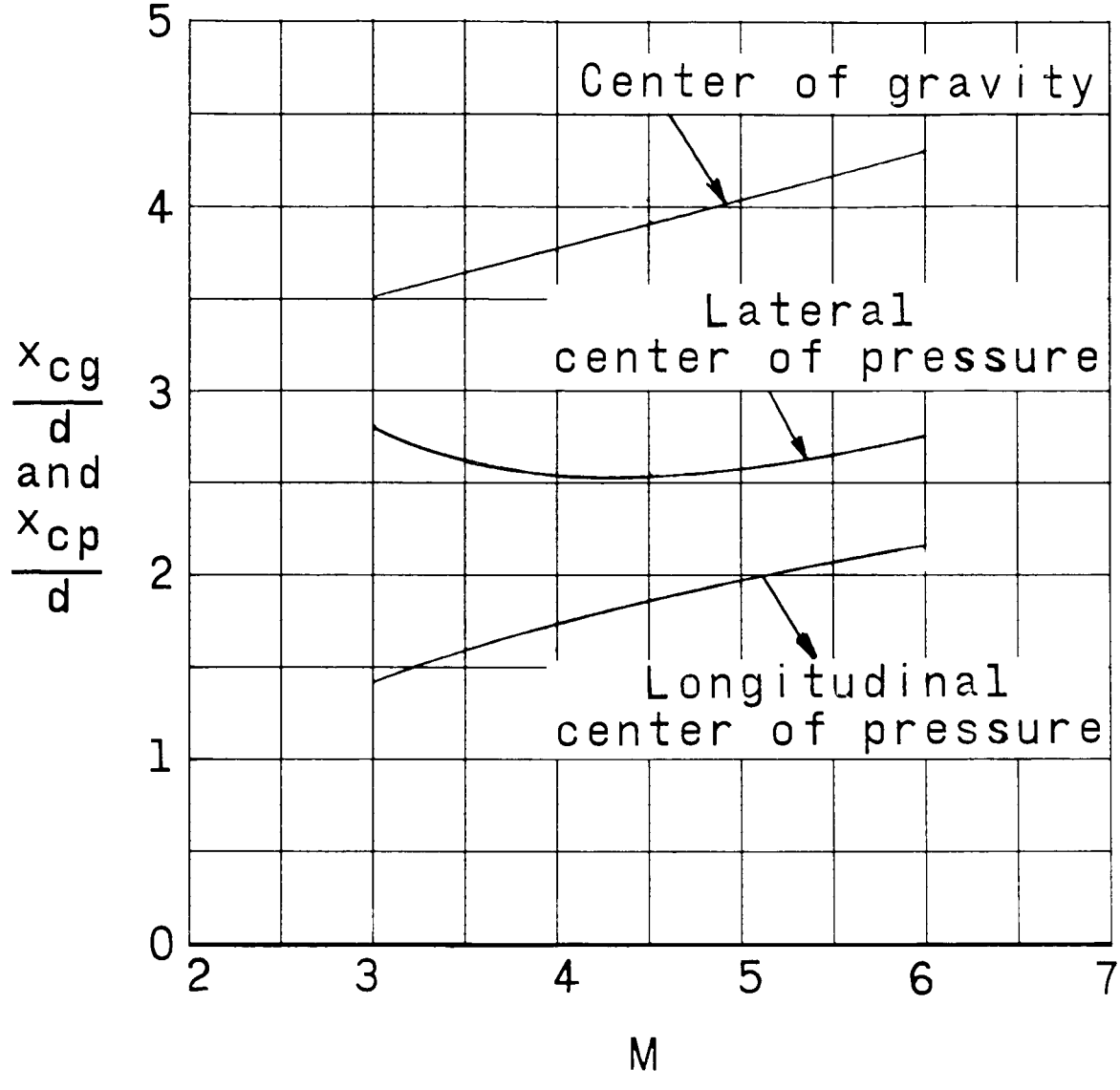

Figure 8.- Comparison of the longitudinal and the lateral center-of-pressure locations for the complete launch vehicle compared with the estimated center-of-gravity location. $\alpha = 0^{0}$.

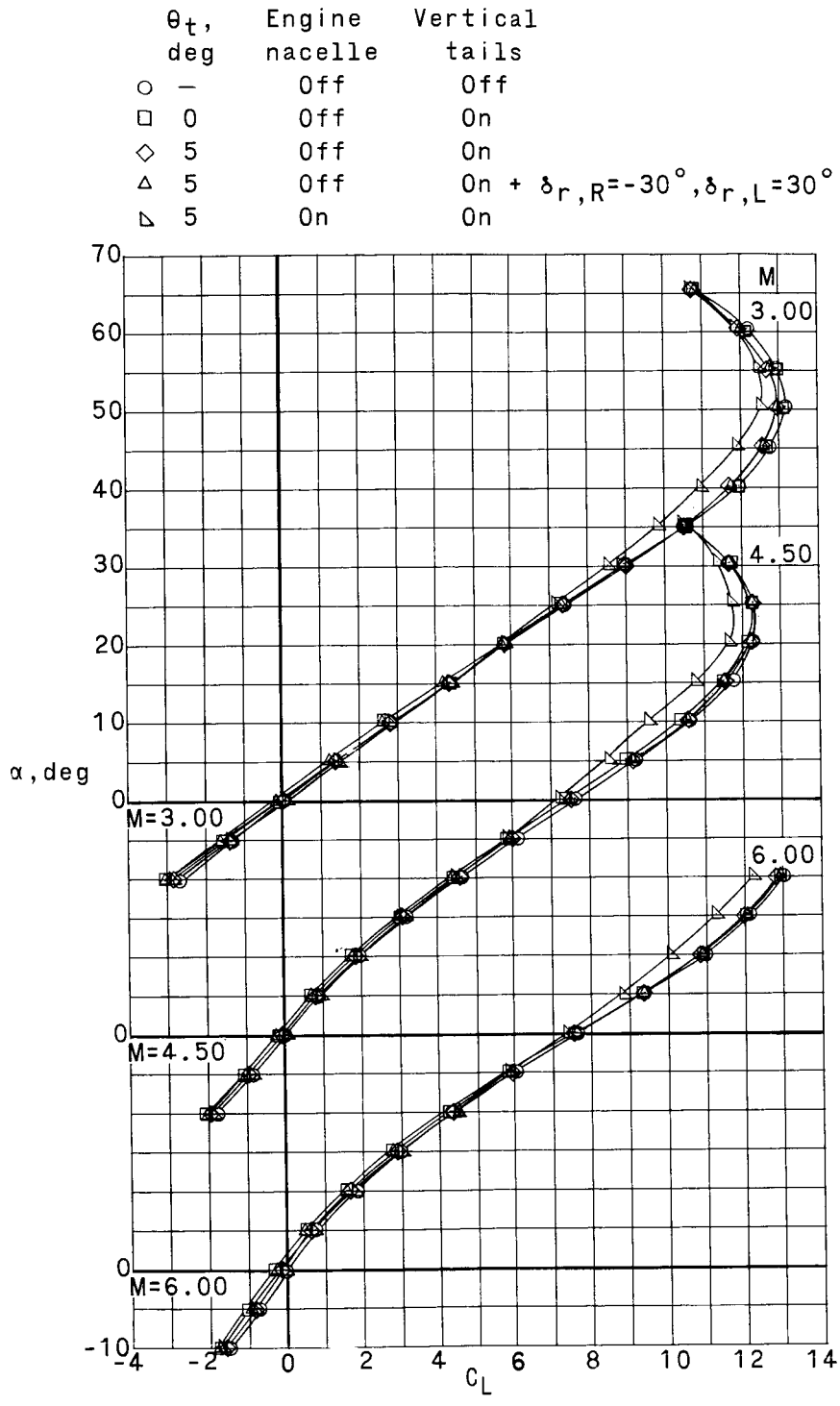

(a) α plotted against C_L.

Figure 9.- Longitudinal aerodynamic characteristics of the winged reusable first stage. $\beta = 0^0$.

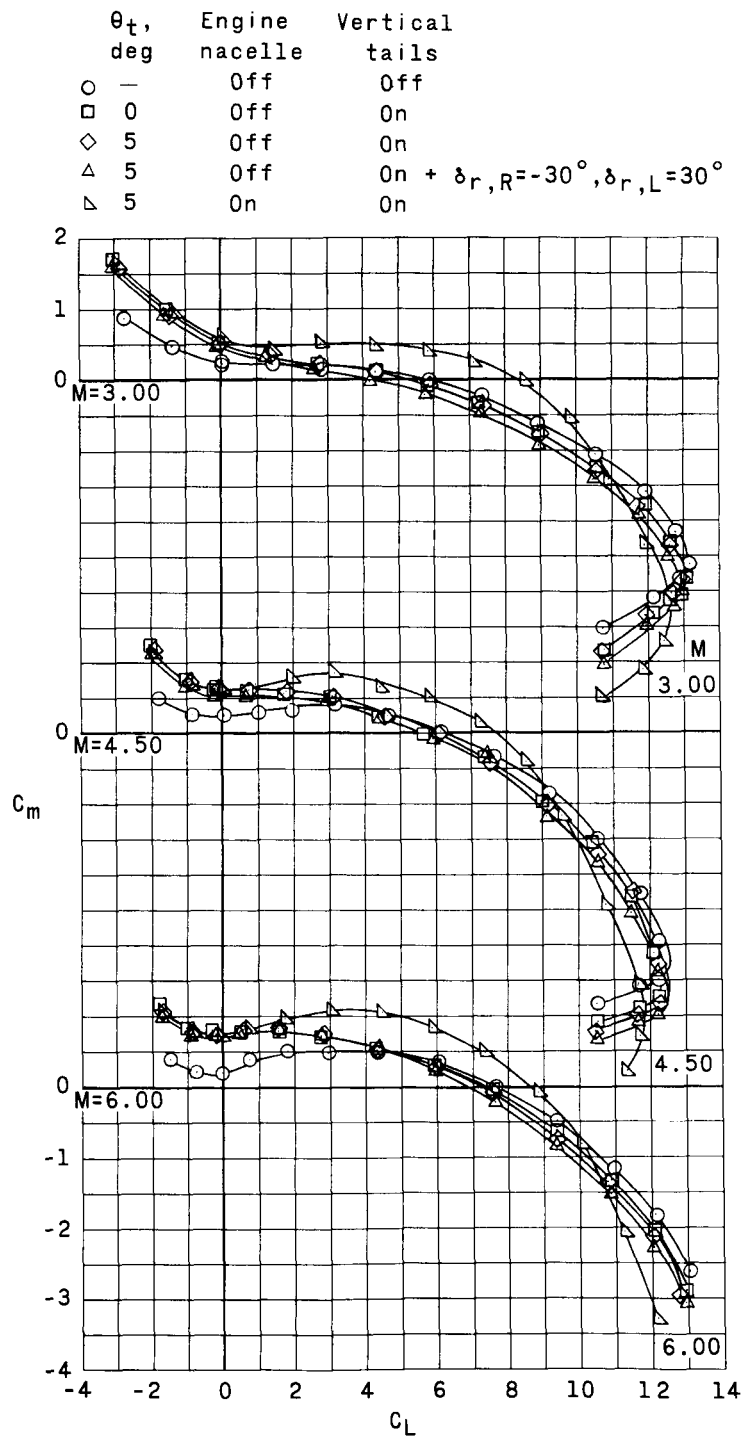

(b) C_m plotted against C_L.

Figure 9.- Continued.

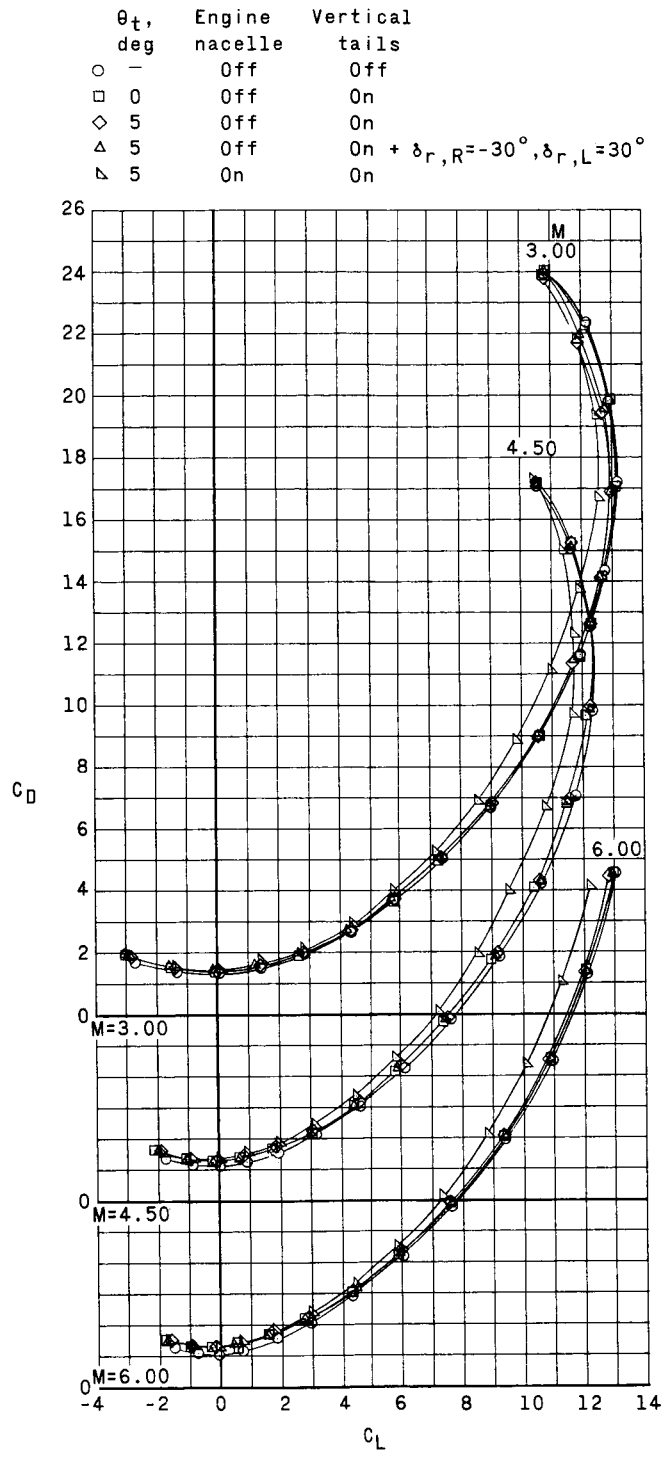

(c) C_D plotted against C_L.

Figure 9.- Continued.

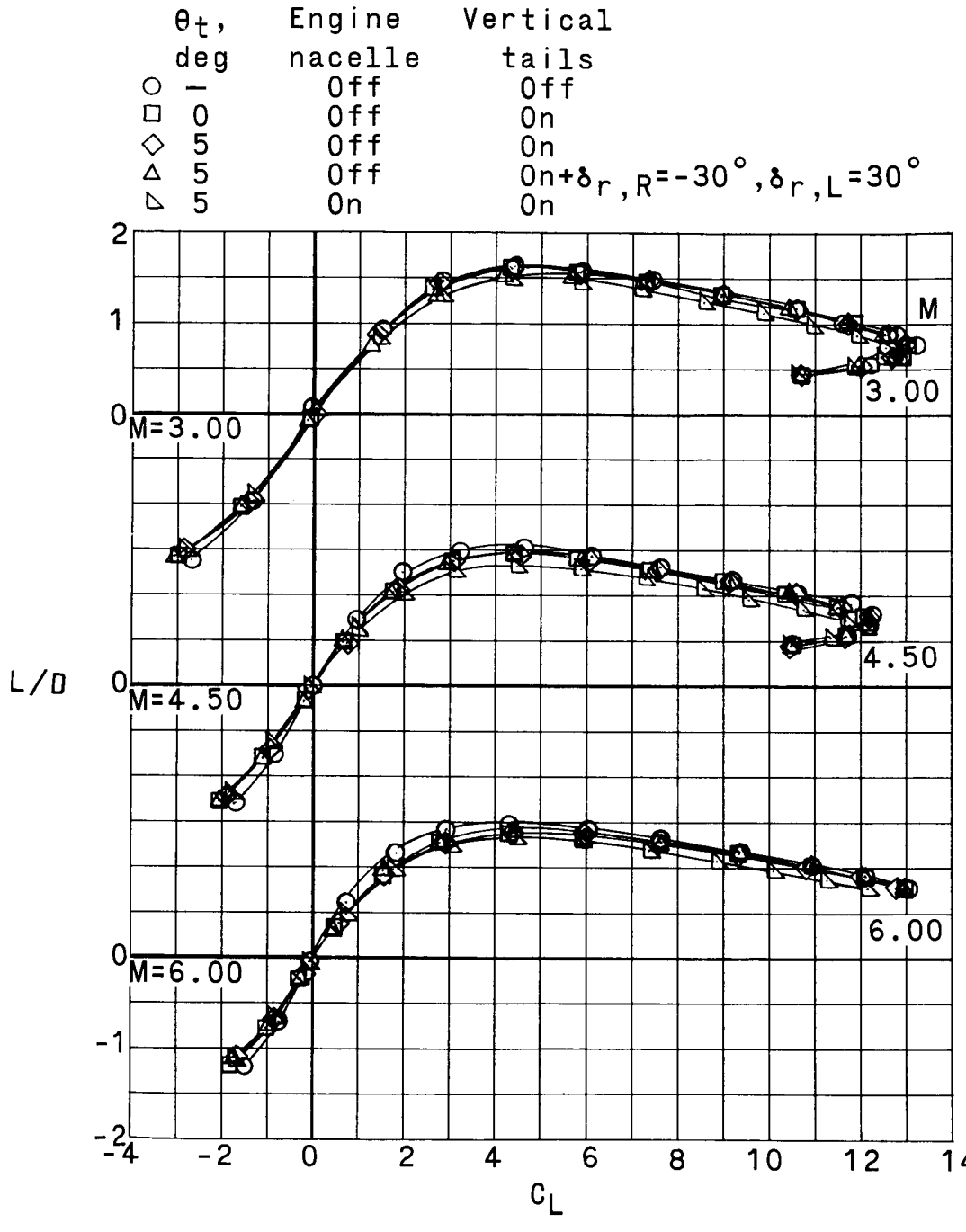

(d) L/D plotted against C_L.

Figure 9.- Concluded.

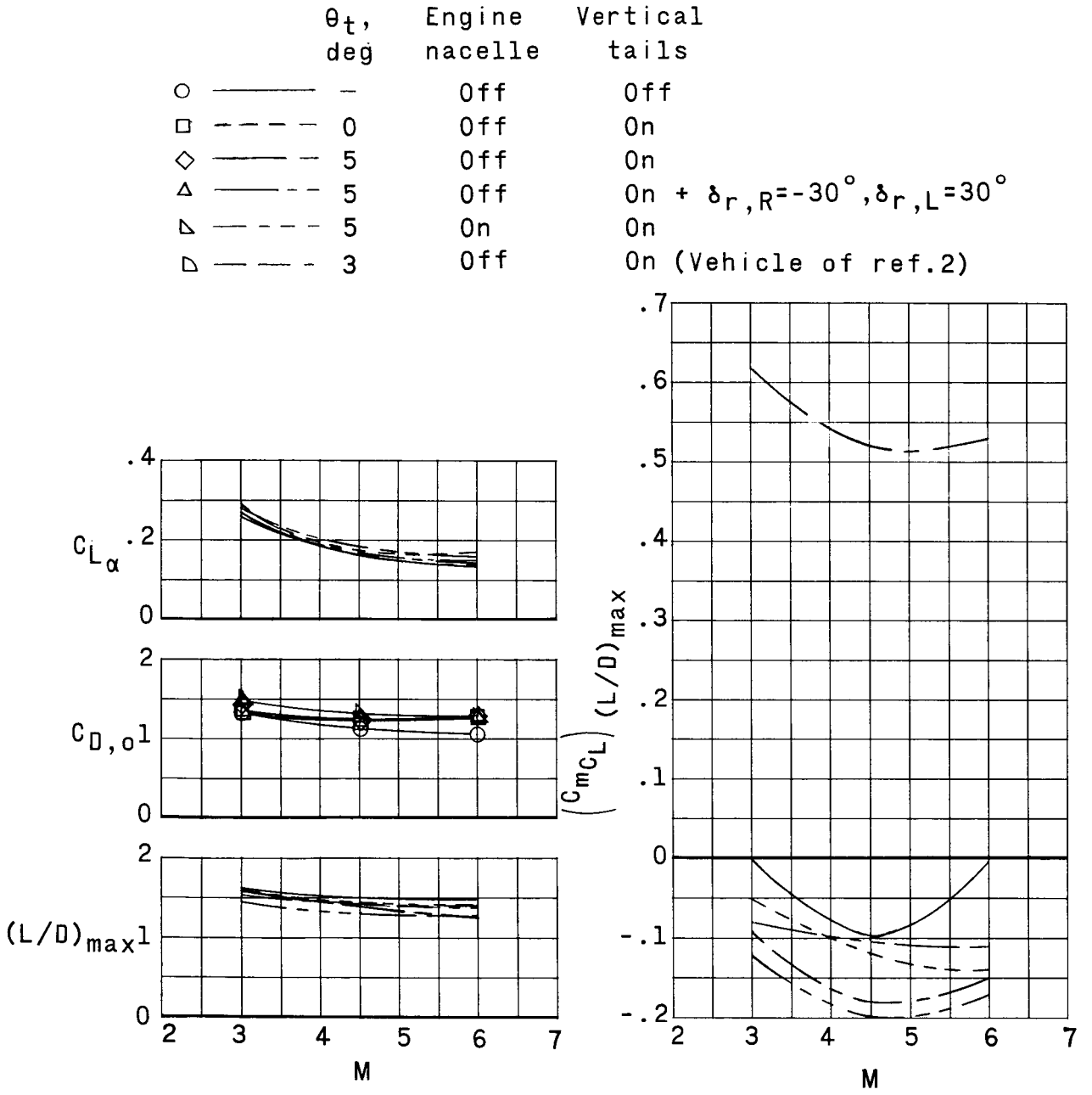

Figure 10.- Variation with Mach number of the longitudinal-stability and drag parameters for the winged reusable first stage. $\beta = 0^{0}$.

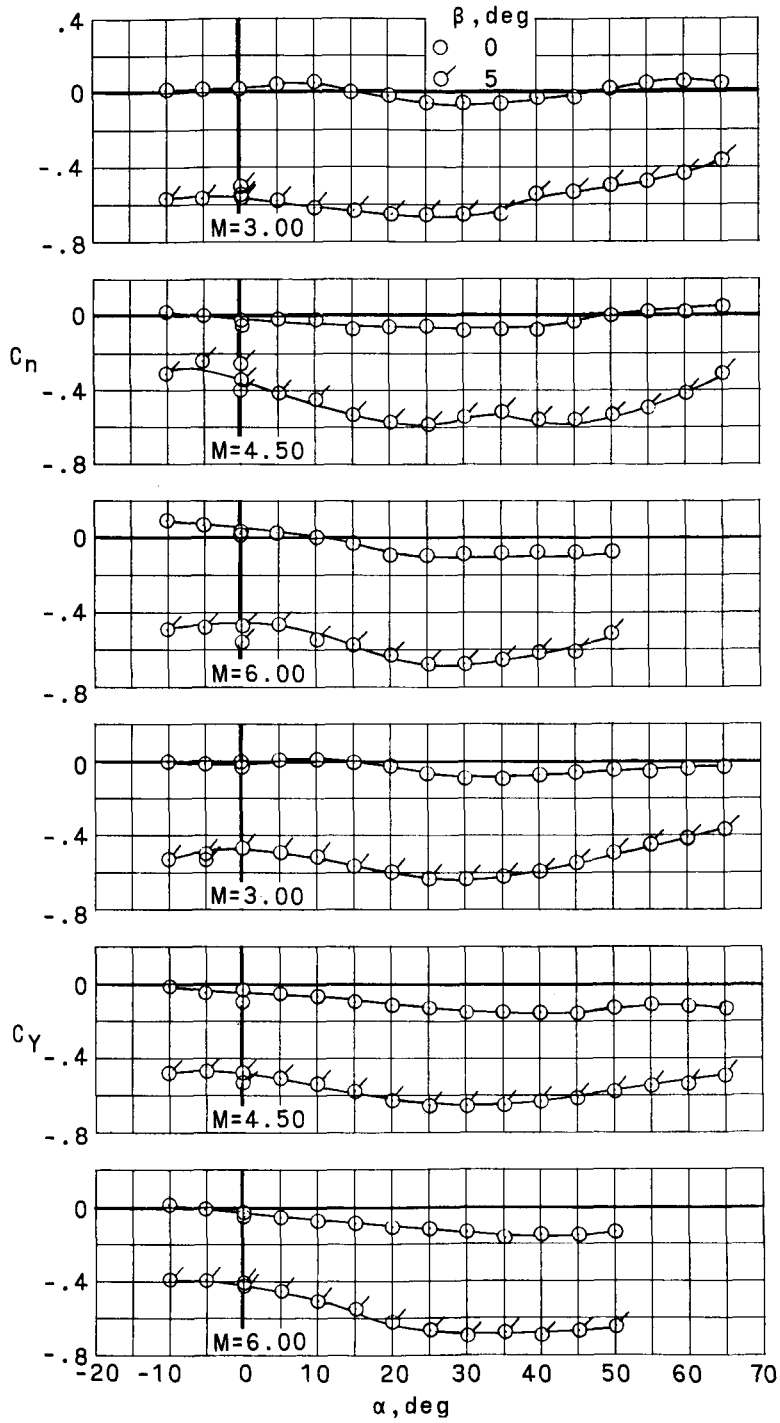

(a) Engine nacelle and vertical tails off.

Figure II.- Lateral aerodynamic characteristics of the winged reusable first stage.

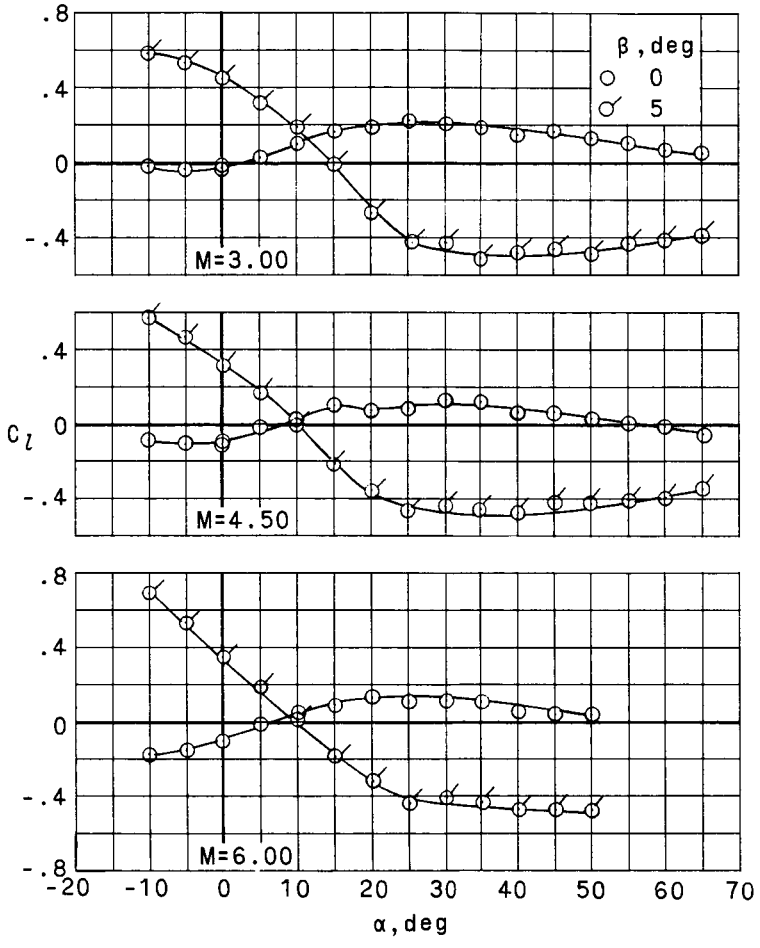

(a) Concluded.

Figure 11.- Continued.

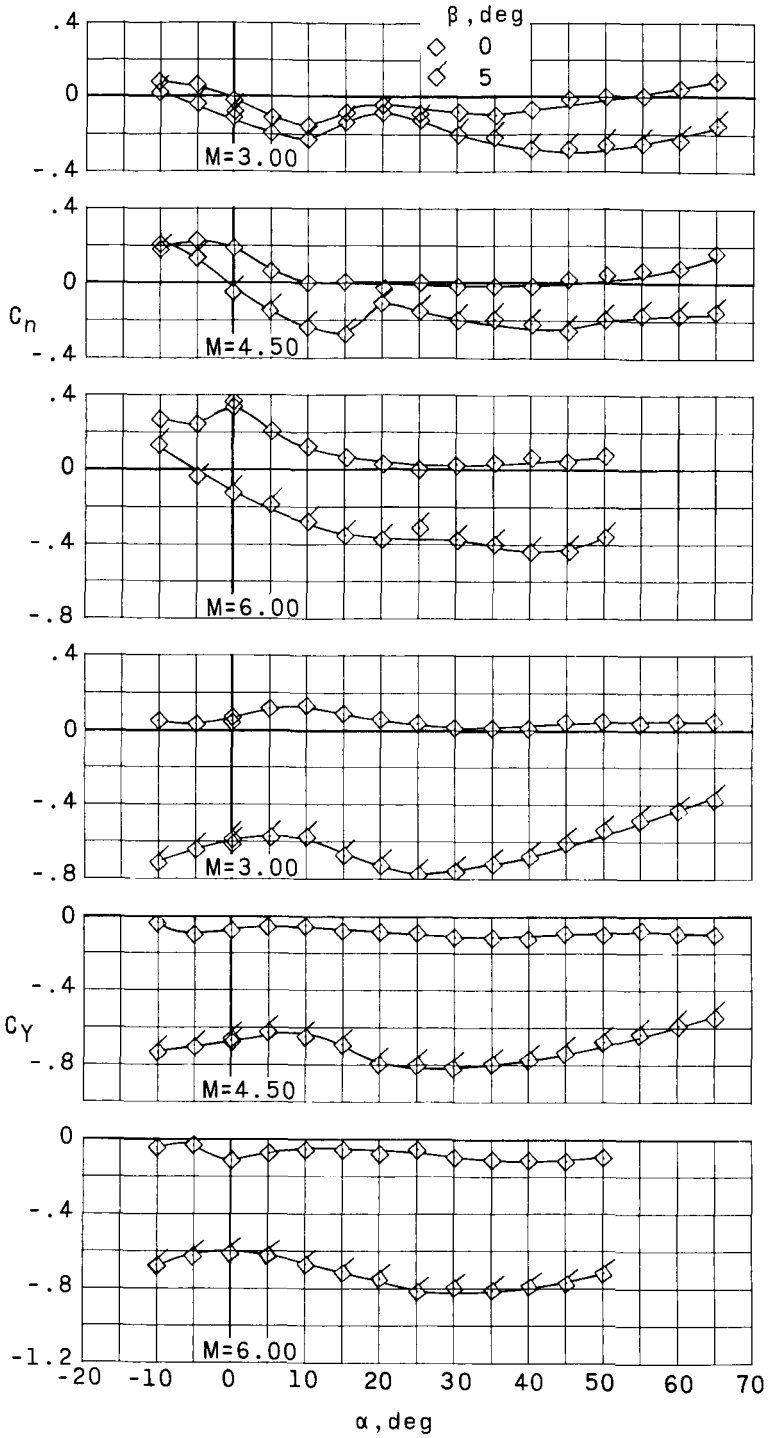

(b) Engine nacelle off; vertical tails on; $\theta_t = 5^0$.

Figure 11.- Continued.

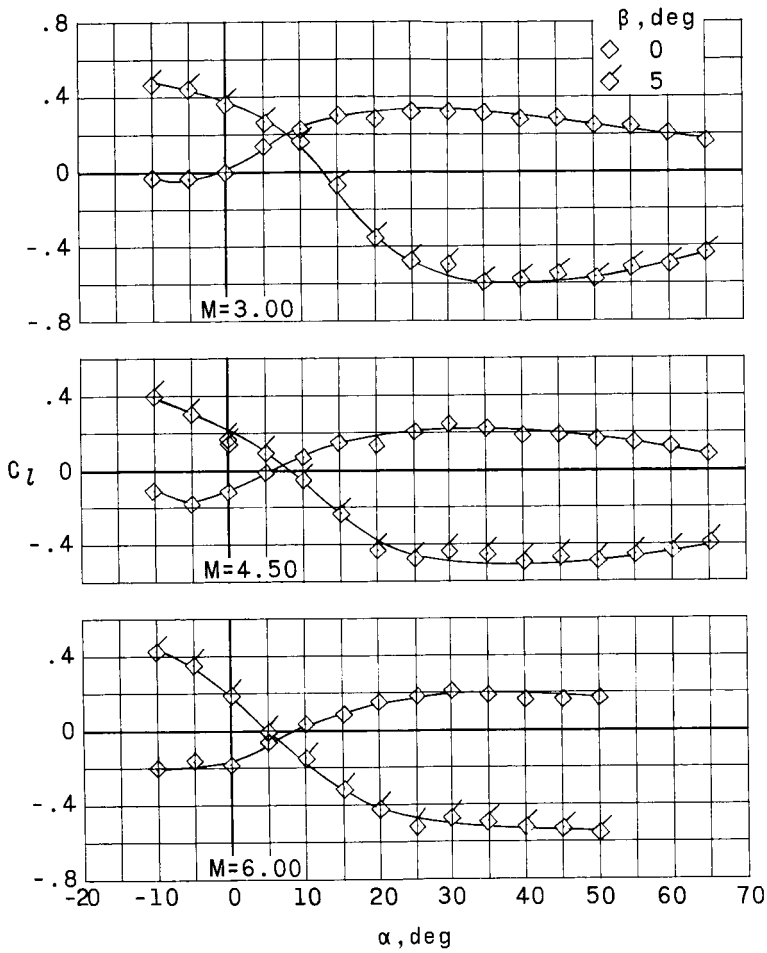

(b) Concluded.

Figure 11.- Continued.

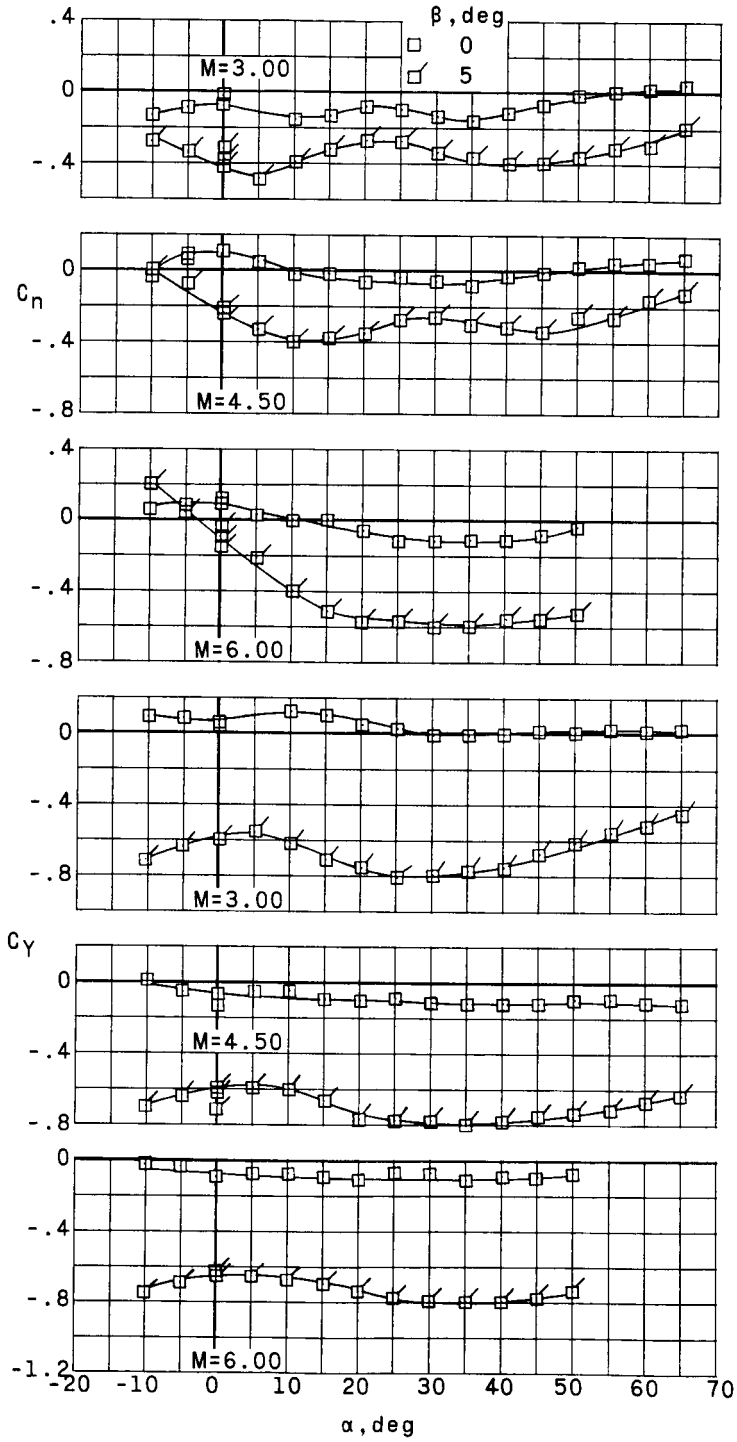

(c) Engine nacelle off; vertical tails on; $\theta_t = 0^0$.

Figure 11.- Continued.

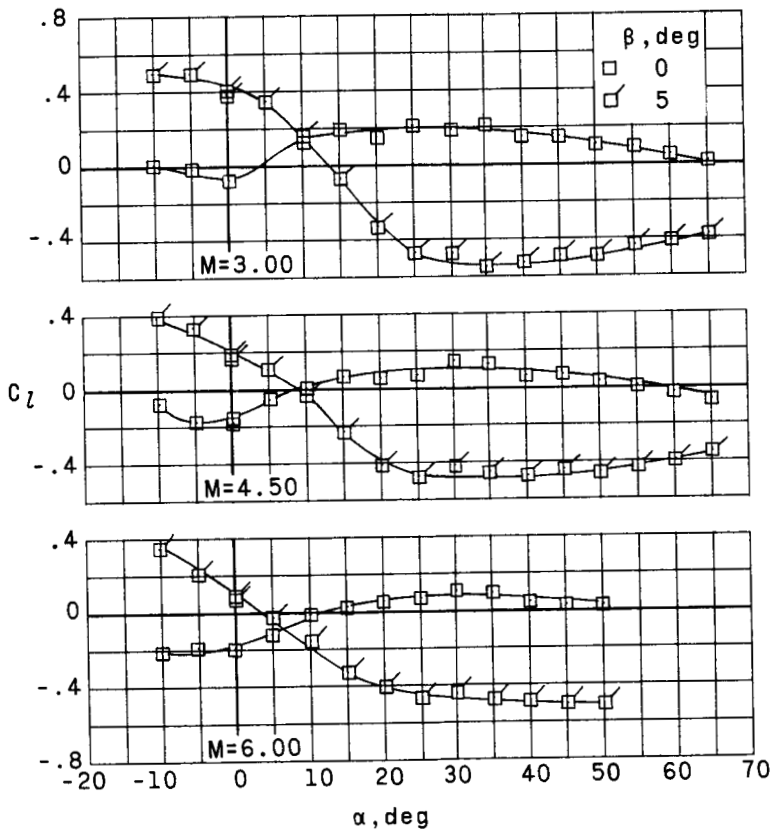

(c) Concluded.

Figure 11.- Continued.

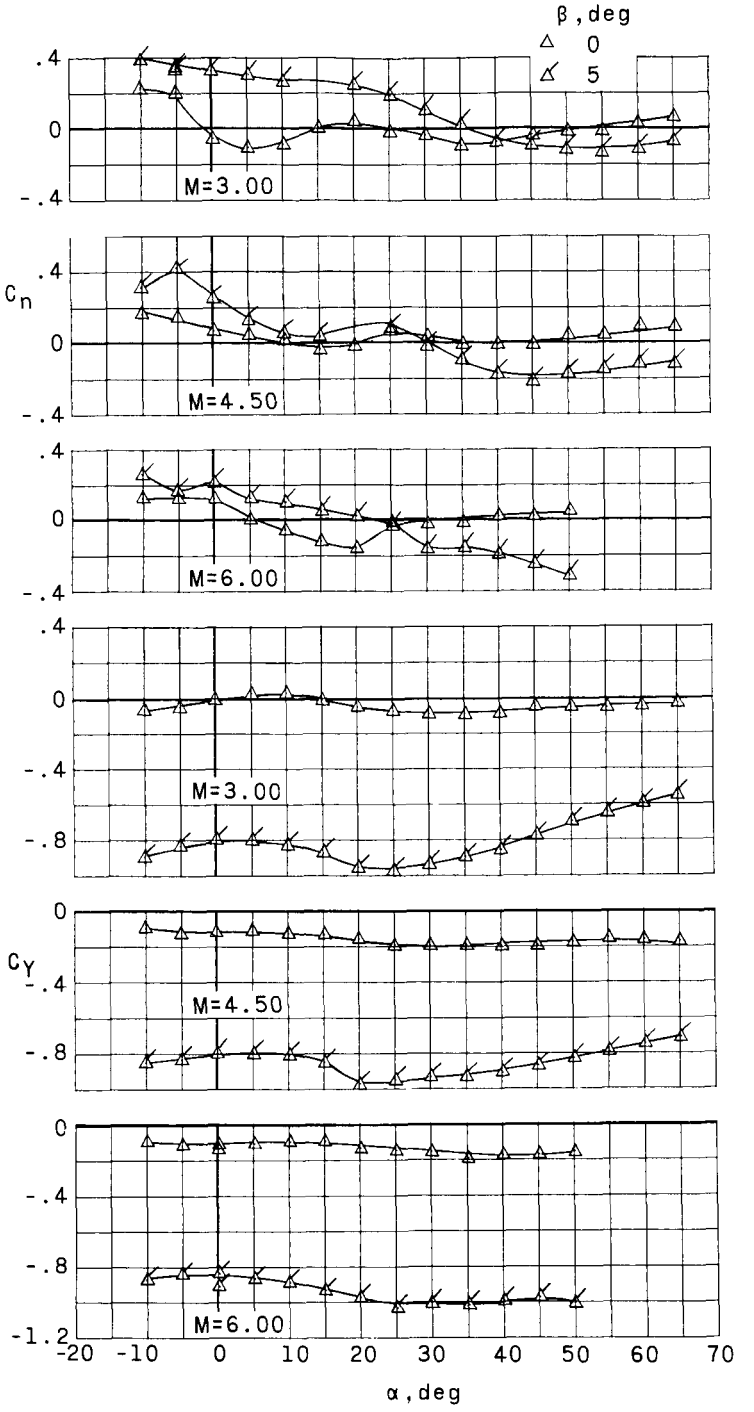

(d) Engine nacelle off; vertical tails on; $\theta_t = 5^0$; $\delta_{r,R} = -30^0$; $\delta_{r,L} = +30^0$.

Figure 11.- Continued.

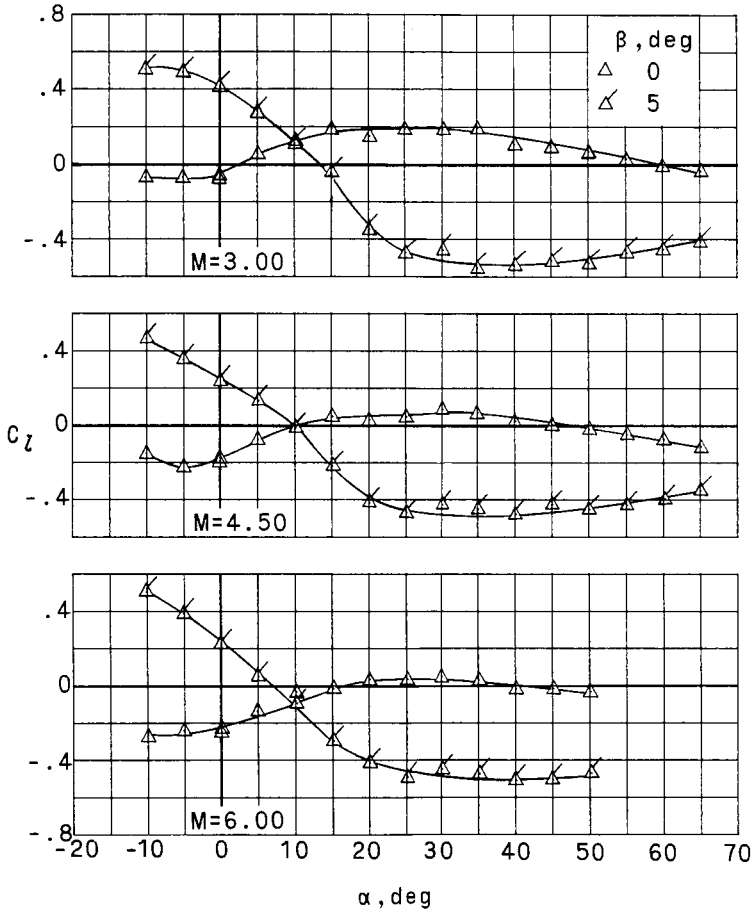

(d) Concluded.

Figure 11.- Concluded.

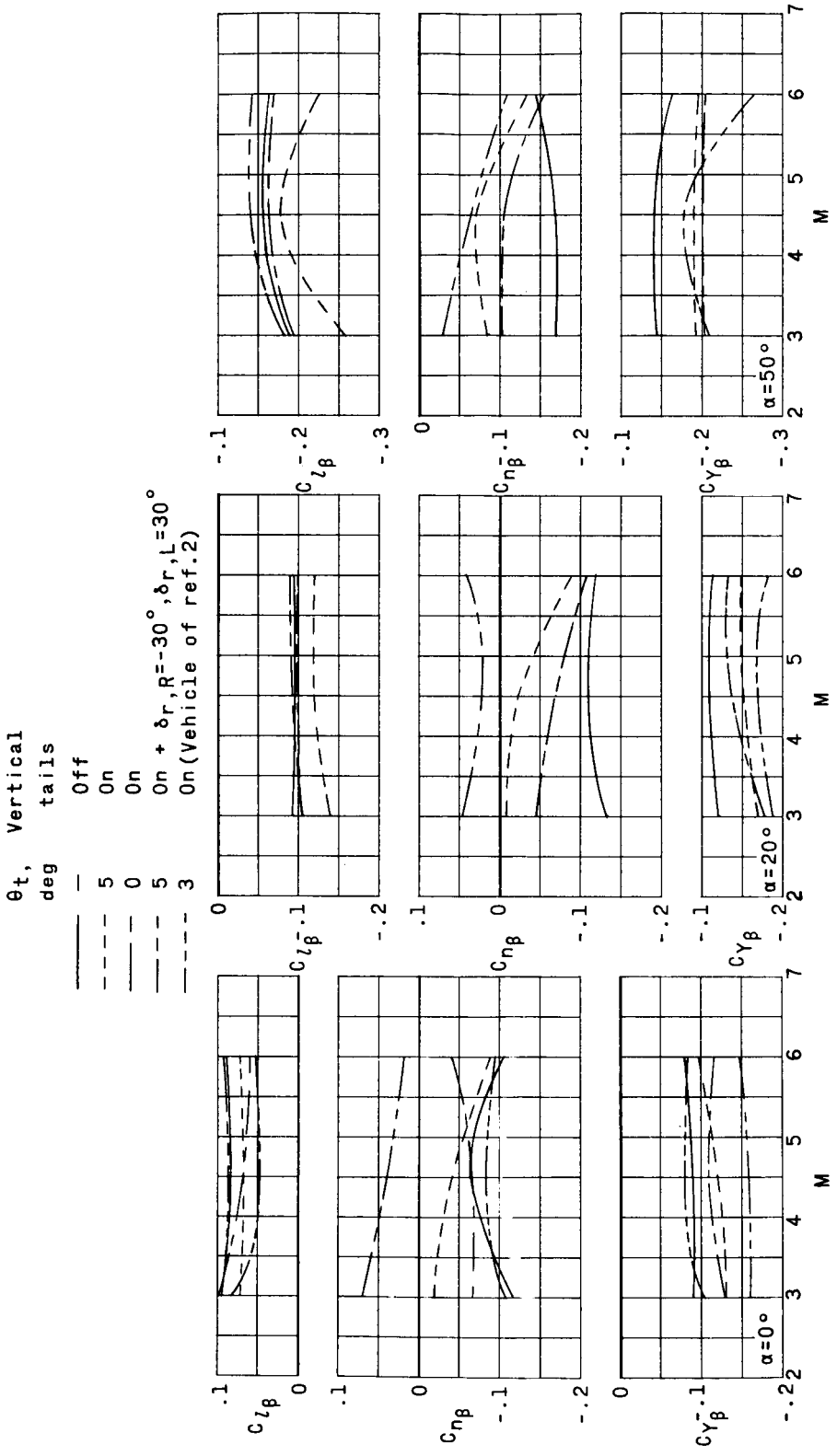

Figure 12.- Variation with Mach number of the lateral-directional-stability parameters for the winged reusable first stage.

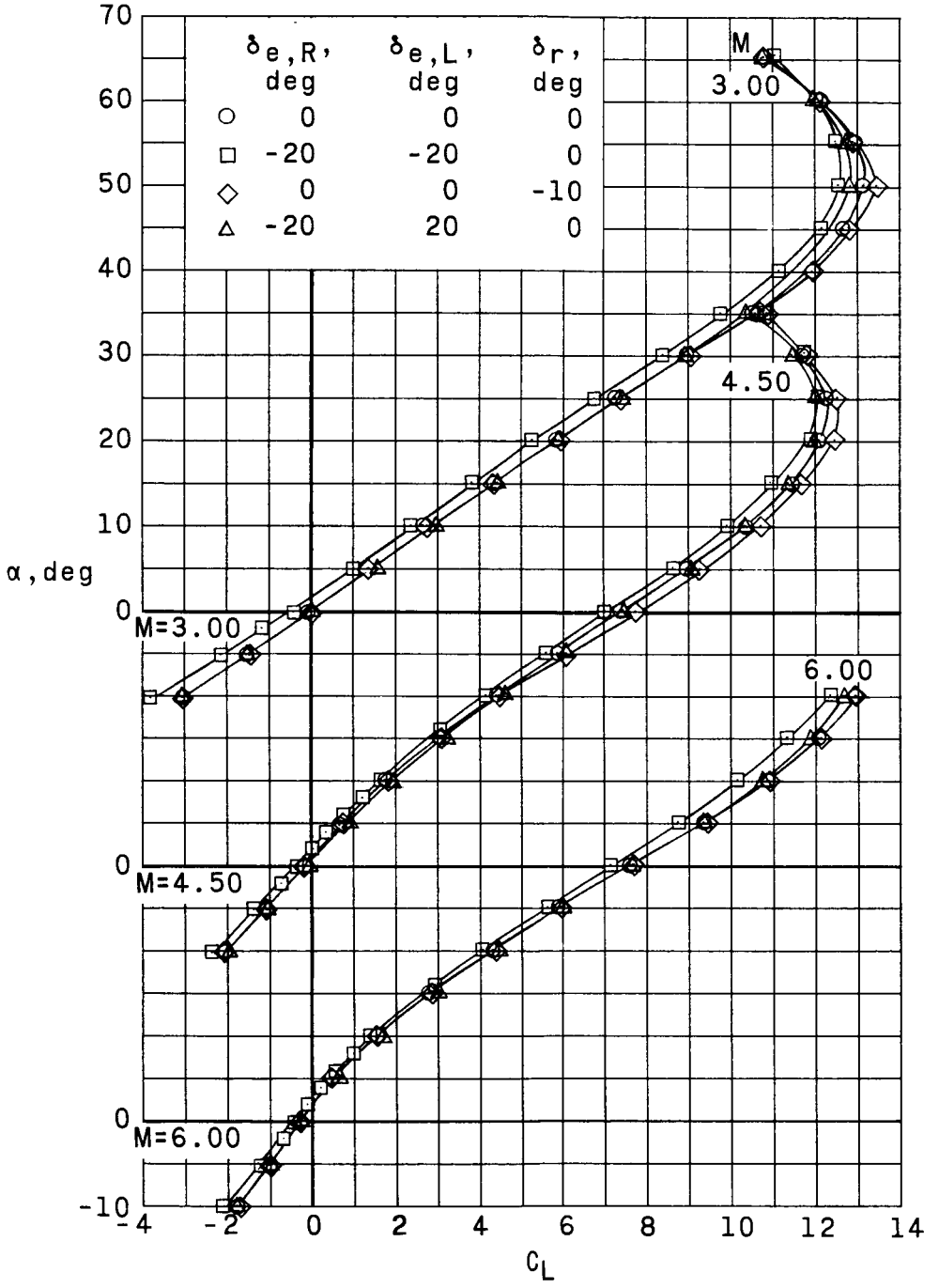

(a) Longitudinal characteristics.

Figure 13.- Aerodynamic characteristics with deflected longitudinal, lateral, and directional control surfaces of the winged reusable first stage. Engine nacelle off; $\theta_t = 0^o$; $\beta = 0^o$.

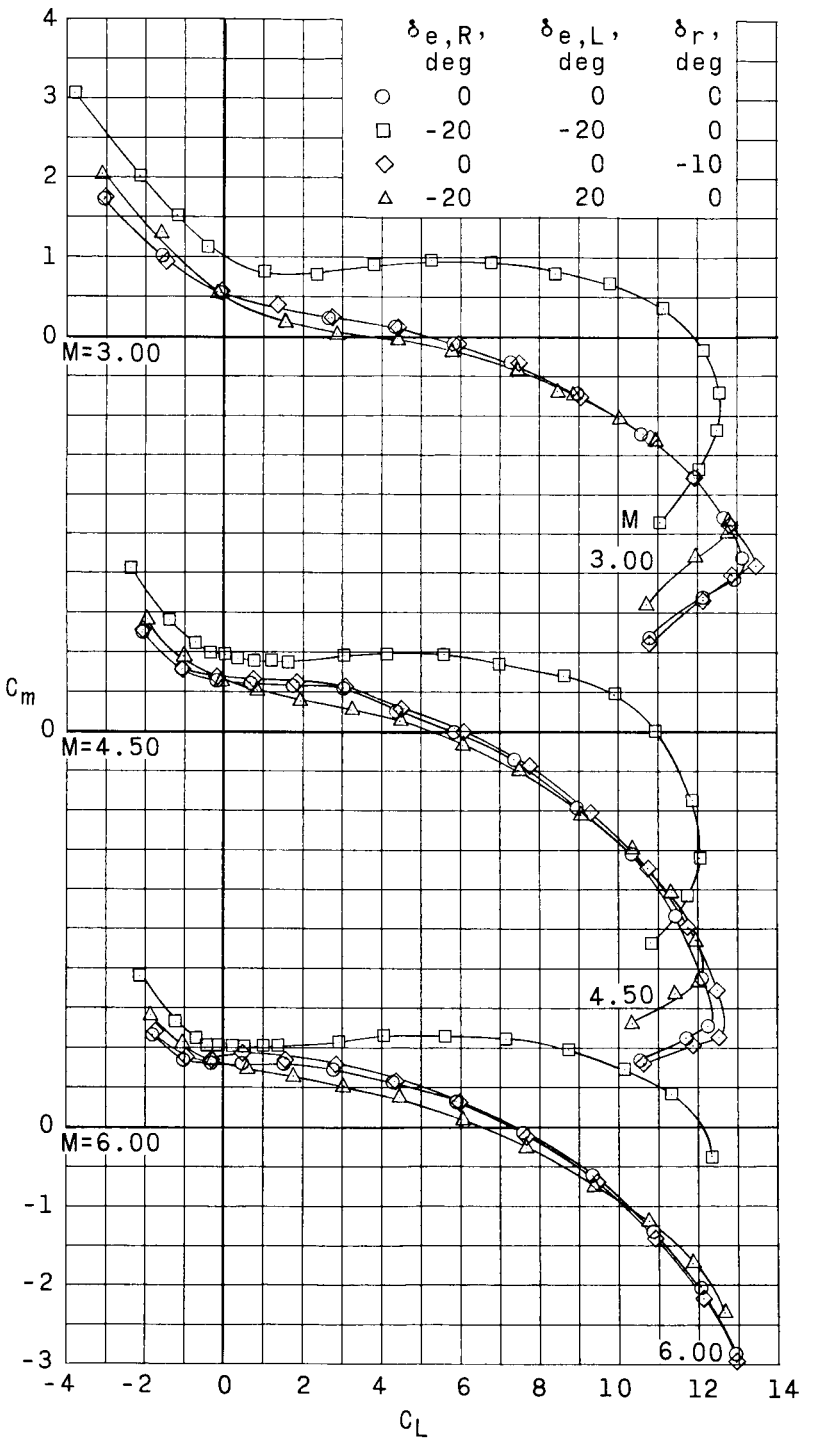

(a) Continued.

Figure 13.- Continued.

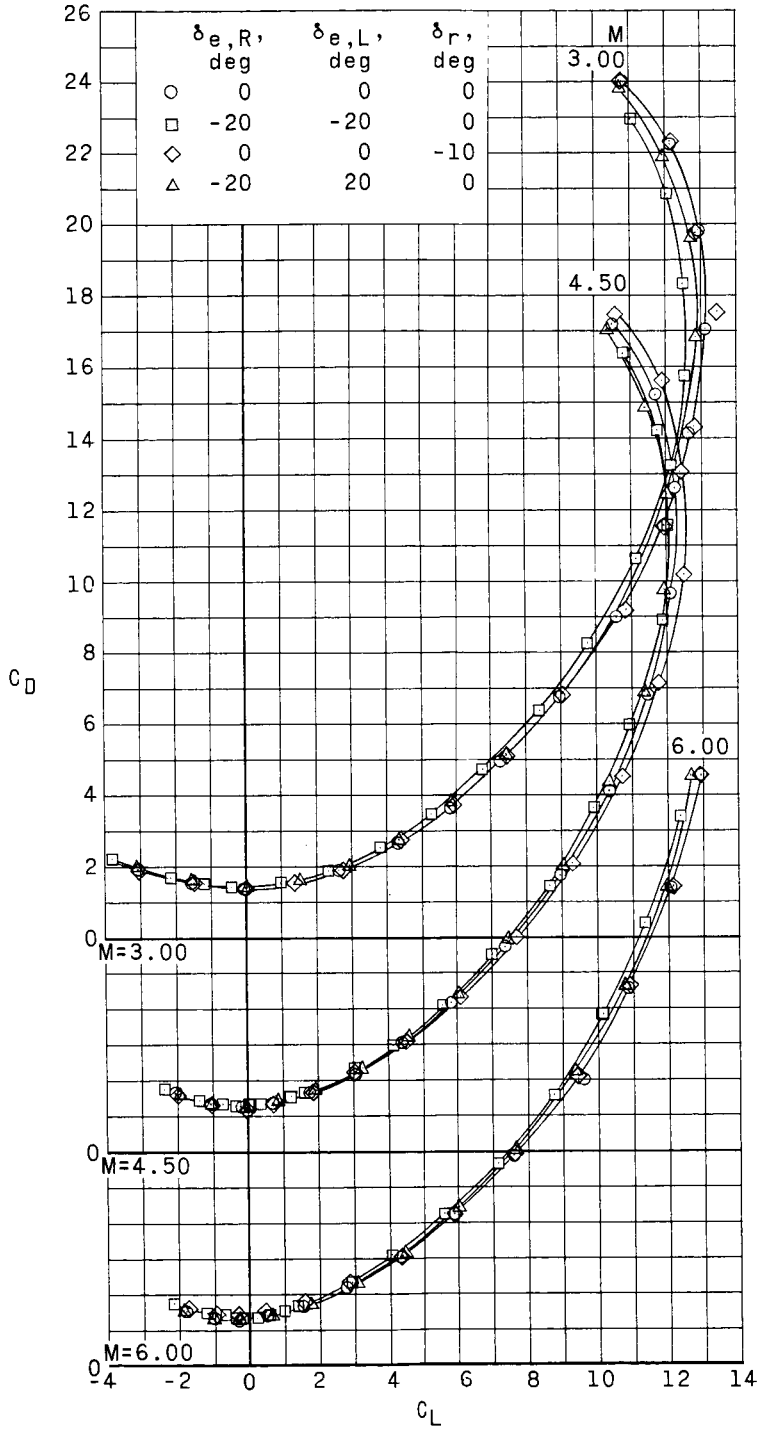

(a) Concluded.

Figure 13.- Continued.

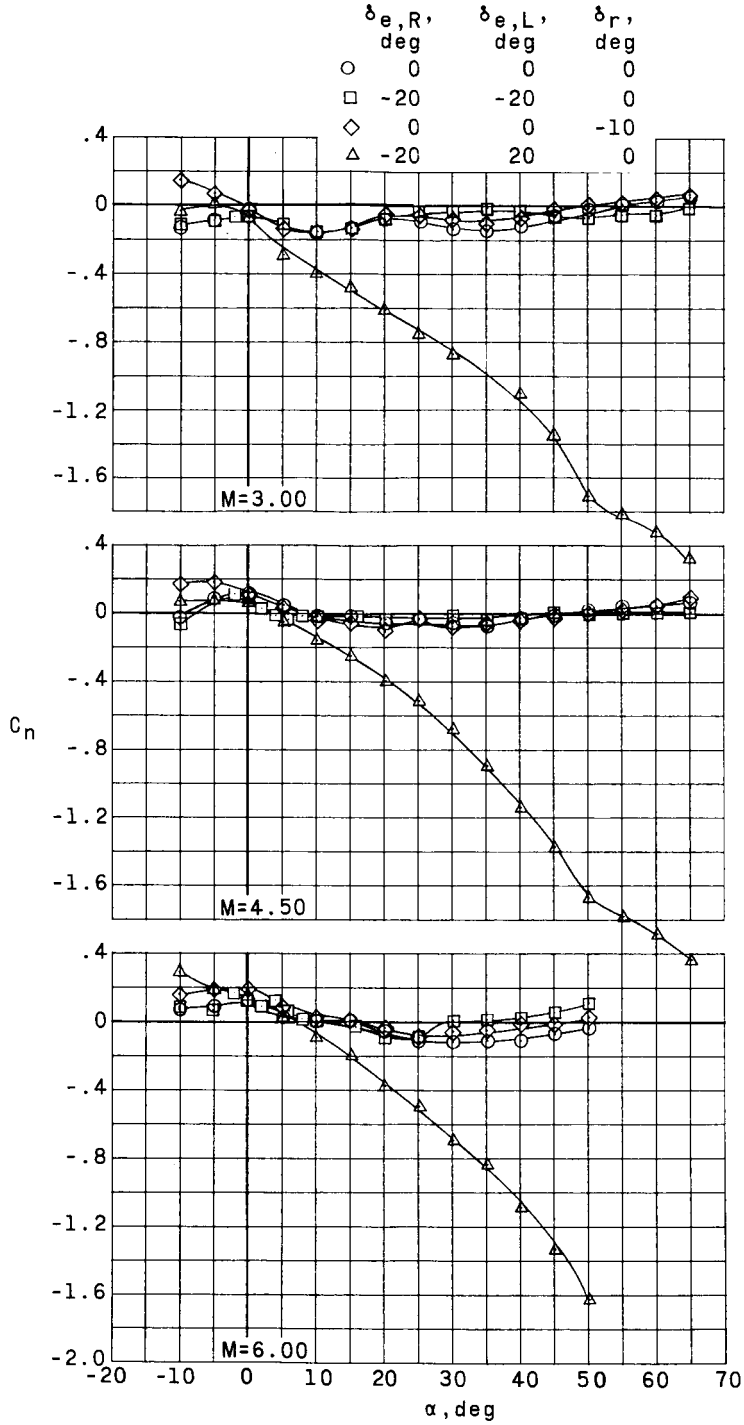

(b) Lateral-directional characteristics.

Figure 13.- Continued.

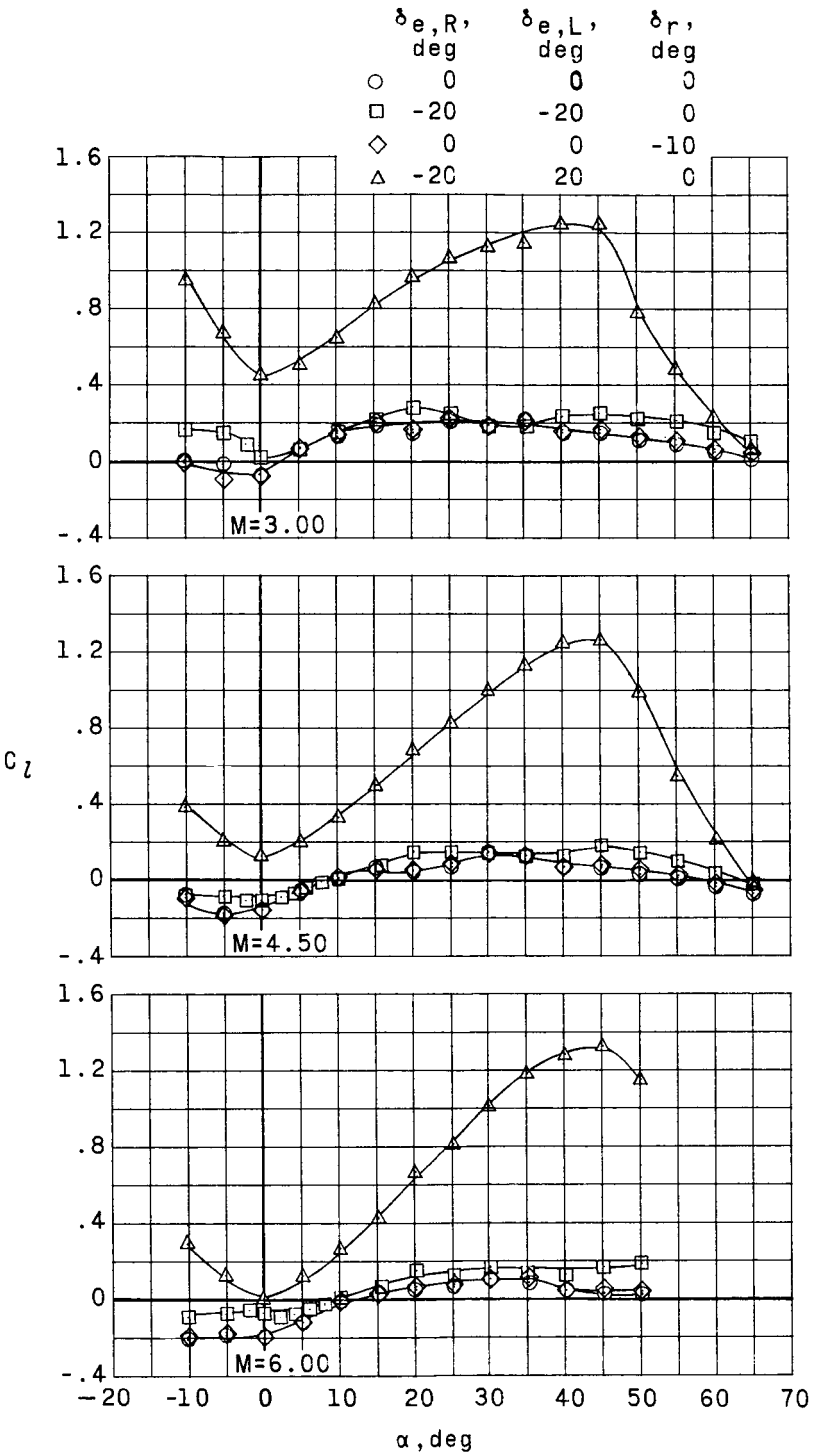

(b) Continued.

Figure 13.- Continued.

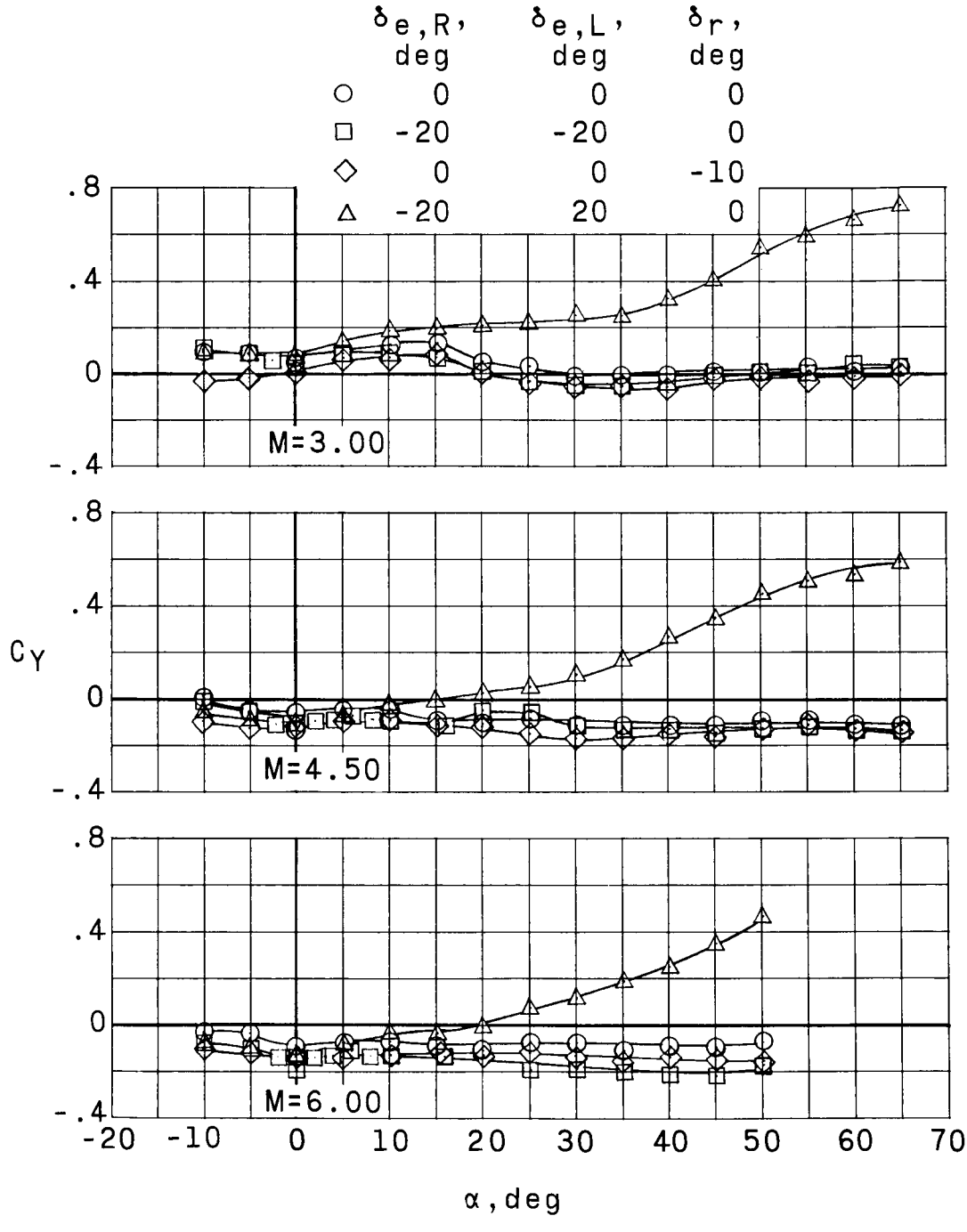

(b) Concluded.

Figure 13.- Concluded.

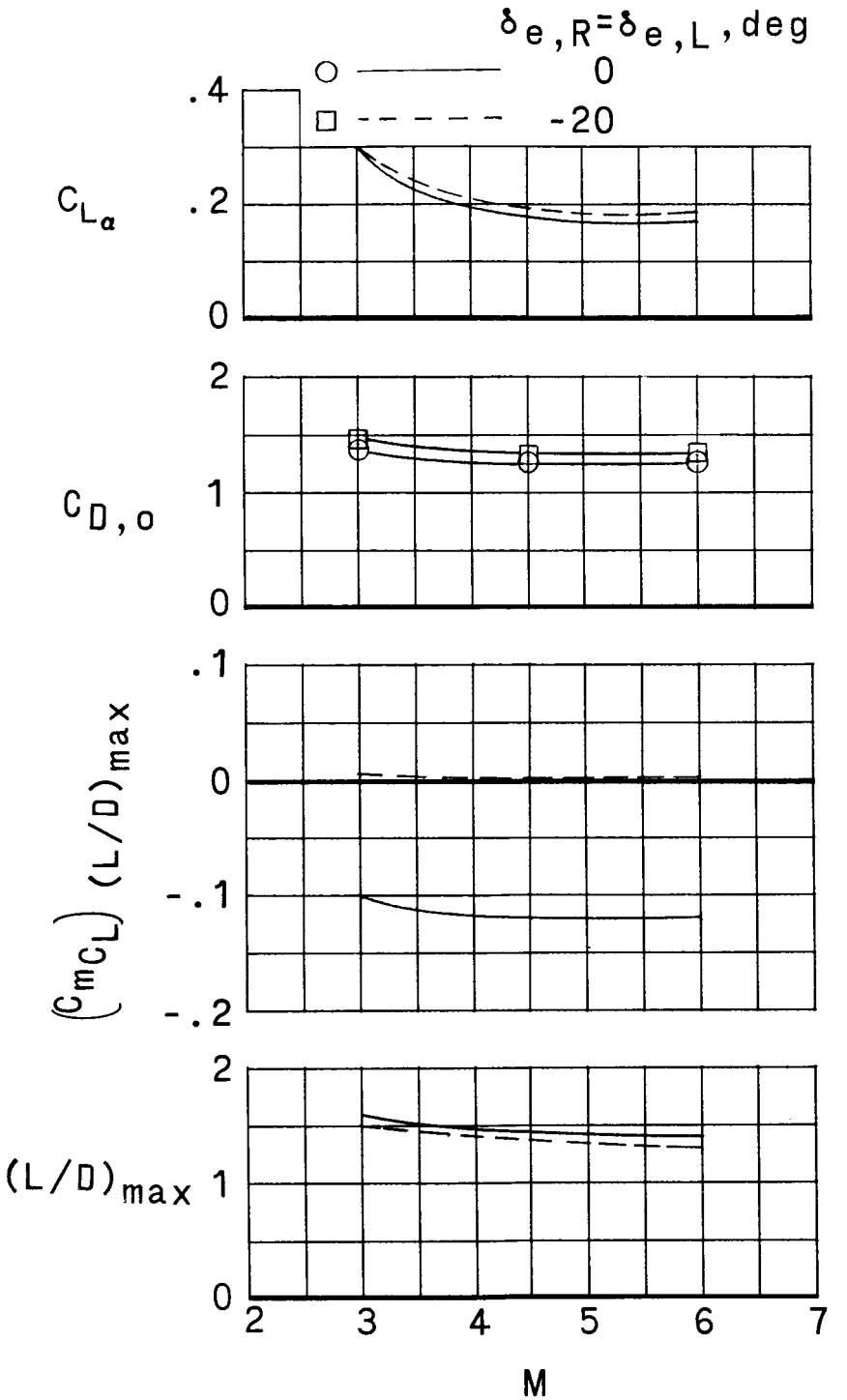

Figure 14.- Variation with Mach number of the longitudinal-stability and drag parameters for the winged reusable first stage showing effects of longitudinal control deflections. Engine nacelle off; $\theta_t = 0^0$; $\beta = 0^0$.

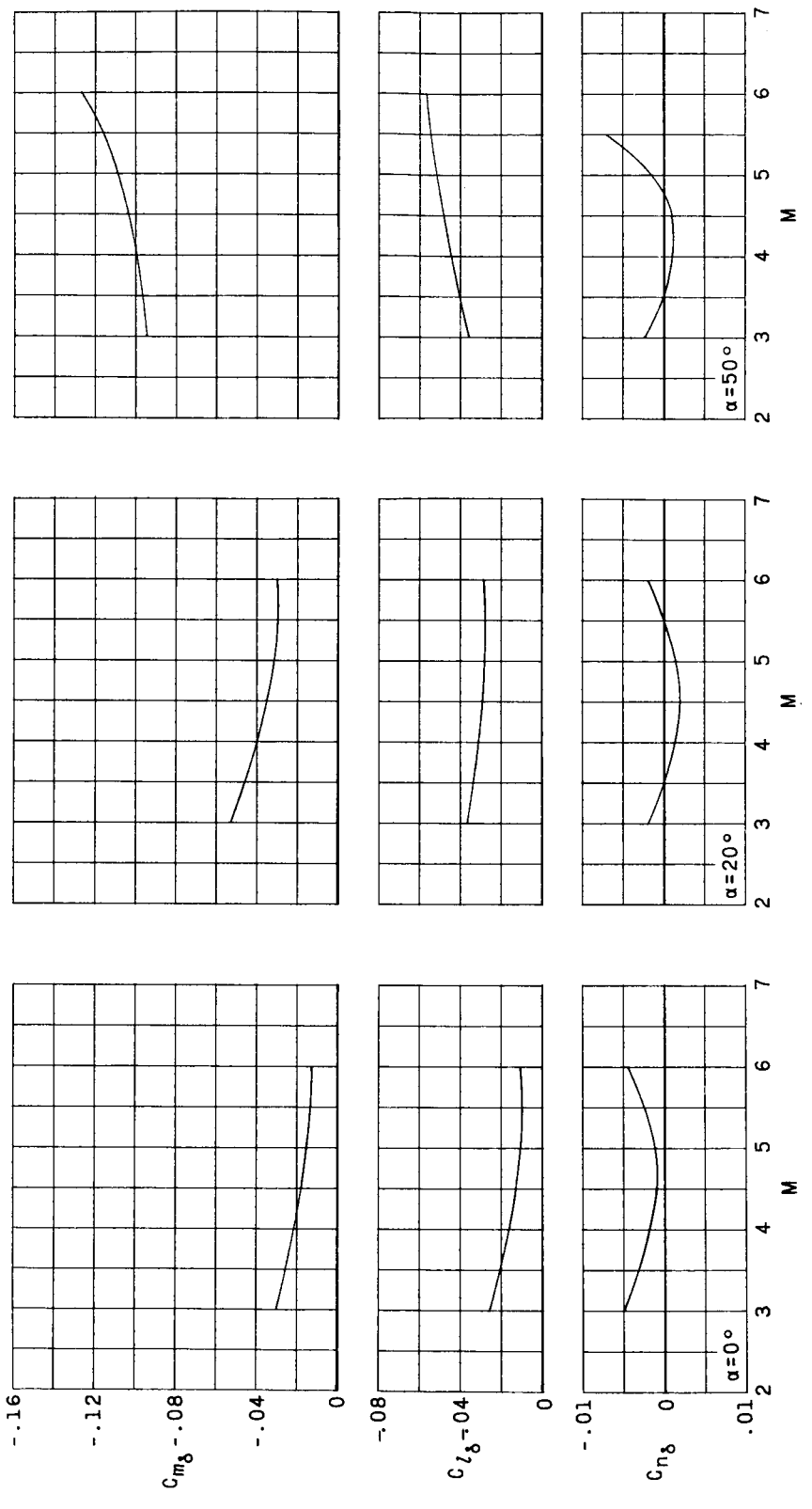

Figure 15.- Control effectiveness of the winged reusable first stage. Engine nacelle off; $\theta_t = 0^0$; $\beta = 0^0$.

"The aeronautical and space activities of the United States shall be conducted so as to contribute . . . to the expansion of human knowledge of phenomena in the atmosphere and space. The Administration shall provide for the widest practicable and appropriate dissemination of information concerning its activities and the results thereof."

—NATIONAL AERONAUTICS AND SPACE ACT OF 1958

NASA SCIENTIFIC AND TECHNICAL PUBLICATIONS

TECHNICAL REPORTS: Scientific and technical information considered important, complete, and a lasting contribution to existing knowledge.

TECHNICAL NOTES: Information less broad in scope but nevertheless of importance as a contribution to existing knowledge.

TECHNICAL MEMORANDUMS: Information receiving limited distribution because of preliminary data, security classification, or other reasons.

CONTRACTOR REPORTS: Technical information generated in connection with a NASA contract or grant and released under NASA auspices.

TECHNICAL TRANSLATIONS: Information published in a foreign language considered to merit NASA distribution in English.

TECHNICAL REPRINTS: Information derived from NASA activities and initially published in the form of journal articles.

SPECIAL PUBLICATIONS: Information derived from or of value to NASA activities but not necessarily reporting the results of individual NASA-programmed scientific efforts. Publications include conference proceedings, monographs, data compilations, handbooks, sourcebooks, and special bibliographies.

Details on the availability of these publications may be obtained from:

SCIENTIFIC AND TECHNICAL INFORMATION DIVISION

NATIONAL AERONAUTICS AND SPACE ADMINISTRATION

Washington, D.C. 20546